Injury-induced BMP signaling negatively regulates *Drosophila* midgut homeostasis

Zheng Guo,[1] Ian Driver,[2] and Benjamin Ohlstein[1]

[1]Department of Genetics and Development and [2]Integrated Program in Cellular, Molecular and Biomedical Studies, Columbia University Medical Center, New York, NY 10032

Although much is known about injury-induced signals that increase rates of *Drosophila melanogaster* midgut intestinal stem cell (ISC) proliferation, it is largely unknown how ISC activity returns to quiescence after injury. In this paper, we show that the bone morphogenetic protein (BMP) signaling pathway has dual functions during midgut homeostasis. Constitutive BMP signaling pathway activation in the middle midgut mediated regional specification by promoting copper cell differentiation. In the anterior and posterior midgut, injury-induced BMP signaling acted autonomously in ISCs to limit proliferation and stem cell number after injury. Loss of BMP signaling pathway members in the midgut epithelium or loss of the BMP signaling ligand *decapentaplegic* from visceral muscle resulted in phenotypes similar to those described for juvenile polyposis syndrome, a human intestinal tumor caused by mutations in BMP signaling pathway components. Our data establish a new link between injury and hyperplasia and may provide insight into how BMP signaling mutations drive formation of human intestinal cancers.

Introduction

In *Drosophila melanogaster*, the adult midgut is maintained by multipotent intestinal stem cells (ISCs) that give rise to a daughter, the enteroblast (EB), which, depending on the level of Notch signaling, will differentiate into an enterocyte (EC) or enteroendocrine cell (Micchelli and Perrimon, 2006; Ohlstein and Spradling, 2006, 2007). When ECs are injured by environmental stressors, JNK and Yki are activated in ECs, which results in expression of Janus kinase–signal transducer and activator of transcription (JAK-STAT) and EGF receptor (EGFR) signaling ligands (Biteau et al., 2008; Jiang et al., 2009, 2011; Buchon et al., 2010; Karpowicz et al., 2010; Shaw et al., 2010; Staley and Irvine, 2010; Biteau and Jasper, 2011). These ligands activate signaling in ISCs and EBs to promote ISC proliferation and EB differentiation (Jiang et al., 2009, 2011; Buchon et al., 2010; Lin et al., 2010; Biteau and Jasper, 2011; Xu et al., 2011). ISC divisions are also regulated by autocrine expression of JAK-STAT ligands (Jiang and Edgar, 2009; Karpowicz et al., 2010; Osman et al., 2012), Yki activation in ISCs (Karpowicz et al., 2010; Shaw et al., 2010), reactive oxygen species (Hochmuth et al., 2011), and activation of the insulin signaling pathway (Amcheslavsky et al., 2009; Choi et al., 2011) in ISC and EBs.

After acute compensation of injury-induced cell loss, stem cells need to rapidly return to preinjurious self-renewal rates to avoid tissue hyperplasia. Indeed, several observations confirm that ISC proliferation rates quickly decrease after removal of noxious stimuli (Jiang et al., 2009; Buchon et al., 2010). Yet, how this dynamic change of division rates is achieved is largely unknown.

Loss-of-function mutations in the bone morphogenetic protein (BMP) receptor type IA and SMAD4 (mother against decapentaplegic [Dpp] homologue 4) are present in a subset of juvenile polyposis (JP) patients (Houlston et al., 1998; Howe et al., 1998, 2001). Furthermore, inhibition of BMP signaling in mouse intestines results in phenotypes that resemble human JP syndrome (Haramis et al., 2004; He et al., 2004), suggesting that BMP signaling in the crypt acts to limit ISC proliferation. Given the similarities between vertebrate and *Drosophila* intestinal homeostasis (Lucchetta and Ohlstein, 2012), the BMP signaling

Correspondence to Benjamin Ohlstein: bo2160@columbia.edu

Abbreviations used in this paper: ACI, after clone induction; ANOVA, analysis of variance; BMP, bone morphogenetic protein; CCR, copper cell region; Dl, Delta; Dpp, decapentaplegic; EB, enteroblast; EC, enterocyte; EGFR, EGF receptor; *esg*, *escargot*; FRT, flippase recognition target; ISC, intestinal stem cell; JAK-STAT, Janus kinase–signal transducer and activator of transcription; JP, juvenile polyposis; MARCM, mosaic analysis with a repressible cell marker; pMad, phosphorylated Mad; RT-qPCR, real-time quantitative PCR; *tkv*, *thick veins*; *tub*, *tubulin*; UAS, upstream activating sequence; *upd*, *unpaired*; vm, visceral muscle; WT, wild type.

The Rockefeller University Press $30.00
J. Cell Biol. Vol. 201 No. 6 945–961
www.jcb.org/cgi/doi/10.1083/jcb.201302049

pathway is an ideal candidate for exploring negative regulation of ISC proliferation.

As is the case with the vertebrate intestine, the *Drosophila* midgut varies along its length in function and cellular identity (Dubreuil, 2004). One of these regions, located in the middle of the midgut, is the copper cell region (CCR). The cells of the CCR are easily identified by their cup-shaped morphology (Filshie et al., 1971). Cells in this region secrete protons that maintain the CCR at low pH (Dubreuil, 2004; Strand and Micchelli, 2011) and are maintained by a population of relatively quiescent ISCs known as gastric stem cells (Strand and Micchelli, 2011). BMP signaling is required during development to establish epithelial expression of the homeotic gene *labial*, which is required for copper cell formation in embryos and larvae (Panganiban et al., 1990; Hoppler and Bienz, 1994; Staehling-Hampton and Hoffmann, 1994). Whether BMP signaling continues to play a role in establishing and maintaining regional identity in the adult midgut has not been established.

Here, we show that in the CCR of the adult *Drosophila* midgut, BMP signaling is constitutive and necessary for copper cell specification. In contrast, in the anterior and posterior midgut, injury-induced signaling regulates the expression of the BMP signaling ligand Dpp in visceral muscle (vm), which then activates the BMP signaling pathway in ISCs to negatively regulate their number and rate of division. Our data provide evidence for how coregulation of antagonistic signals mediate tissue homeostasis and how disconnect between these signals can lead to abnormal tissue homeostasis.

Results

BMP signaling promotes adult *Drosophila* copper cell specification

To determine the extent of active BMP signaling in the adult midgut, we examined the expression patterns of two markers of BMP signaling: (1) *Dad-lacZ* (Tsuneizumi et al., 1997) and (2) phosphorylated Mad (pMad; König et al., 2011). *Dad-lacZ* expression could be detected in the anterior and posterior midgut but was consistently expressed at high levels in and adjacent to the middle part of the midgut known as the CCR, a region delineated by expression of Labial, a CCR marker (Fig. 1 A; Chouinard and Kaufman, 1991; Strand and Micchelli, 2011). To determine in which cells of the CCR BMP signaling was active, we costained midguts for *Dad-lacZ* or pMad and markers of copper cells (Labial; Fig. 1, B and B′), gastric stem cells and EBs (*escargot* [*esg*]-GFP, a GFP protein trap in the *esg* gene; Fig. 1, C and C′; Micchelli and Perrimon, 2006; Buszczak et al., 2007), and enteroendocrine cells (Prospero; Fig. S1, A–A″; Micchelli and Perrimon, 2006; Ohlstein and Spradling, 2006). In all cases, *Dad-lacZ* or pMad was coexpressed with Labial, *esg*-GFP, and Prospero, demonstrating that BMP signaling is constitutively active in all epithelial cells of the CCR.

To identify a role for BMP signaling in the CCR, we made positively marked null mutant mosaic analysis with a repressible cell marker (MARCM; Lee and Luo, 1999) clones of two members of the BMP signaling pathway, *thick veins* (*tkv*; tkv^{8}) and *Mad* (Mad^{12}). pMad staining was absent from tkv^{8} clones in the CCR (Fig. 1, D and D′), whereas *Dad-lacZ* staining was absent from Mad^{12} clones in the CCR (Fig. 1, E and E′), demonstrating that the pMad antibody and *Dad-lacZ* enhancer we used were specific reporters of BMP signaling in the CCR. Mutant nuclei were small and tightly packed, unlike wild-type (WT) copper cell nuclei, which are polyploid and regularly spaced (Fig. 1, E, E′, G, and G′; Hoppler and Bienz, 1994). Because the gene *labial* is necessary for copper cell identity in embryonic and larval midguts (Hoppler and Bienz, 1994), we stained the CCR for Labial. Although cells outside of the clone expressed Labial, Labial was undetectable within tkv^{8} and Mad^{12} clones (Fig. 1, F–G′). Expression of GFP by the temperature-inducible ISC–EB driver *esg*-Gal4 *tubulin* (*tub*)-Gal80^{ts} (esg^{ts}) had no effect on expression of Labial (Fig. S1 B). In contrast, knockdown of BMP signaling in the CCR using esg^{ts} to drive expression of *tkv* or *Mad* RNAi (Fig. S1, C and D) or the ISC driver *Delta* (*Dl*)-Gal4 (Fig. S1 E) to drive expression of *Mad* RNAi (Fig. S1 F) for 9 d at the permissive temperature (30°C) led to nearly complete loss of Labial expression.

Copper cells secrete protons into the lumen of the CCR (Dubreuil et al., 1998; Dubreuil, 2004), lowering the local pH of the midgut. We knocked down BMP signaling in the CCR using esg^{ts} to drive expression of *Mad* or *tkv* RNAi for 9 d at 30°C and fed animals food containing bromophenol blue dye, a chemical indicator of midgut pH (Shanbhag and Tripathi, 2009). In control midguts, dye color was blue, pH > 4.6, in the anterior and posterior midgut and yellow, pH < 3.0, in the CCR (Fig. 1 H). In esg^{ts}>*tkv* RNAi (Fig. 1 I) or esg^{ts}>*Mad* RNAi midguts (Fig. S1 G), dye color was blue throughout the midgut, demonstrating that functional copper cells were not made. Thus, our data demonstrate that copper cells cannot be generated when BMP signaling is compromised in progenitor cells.

Midgut injury up-regulates BMP signaling

Comparing *Dad-lacZ* expression and pMad staining in multiple midguts, we found that in contrast to the CCR, BMP signaling in the anterior and posterior midgut varied greatly from midgut to midgut (Fig. 2 A, compare with Fig. 1 A and Fig. S2 A). We hypothesized that this variable pattern reflected the variation in local injury that the midgut is exposed to from bacteria and the digestive process (Buchon et al., 2009; Chatterjee and Ip, 2009; Jiang et al., 2009) and reasoned that extensive injury to the midgut should lead to a dramatic up-regulation of BMP signaling throughout the entire midgut. Because feeding bleomycin to animals results in widespread EC death (Amcheslavsky et al., 2009), we reared animals on control food or food containing bleomycin for 24 h and, immediately after, determined the expression of *Dad-lacZ*, pMad, and *upd3*-Gal4 upstream activating sequence (UAS)-GFP (*upd3*>GFP), a marker of damaged midgut cells (Jiang et al., 2009). In midguts from animals reared on control food, expression of *upd3*>GFP and *Dad-lacZ* was mostly limited to the CCR and part of the posterior midgut (Fig. S2, B and B′). In contrast, in midguts from animals fed bleomycin, the expression of all three reporters became broadly detectable (Fig. 2, B–C′). Similar results were obtained by feeding flies *Ecc15* (*Erwinia carotovora carotovora*

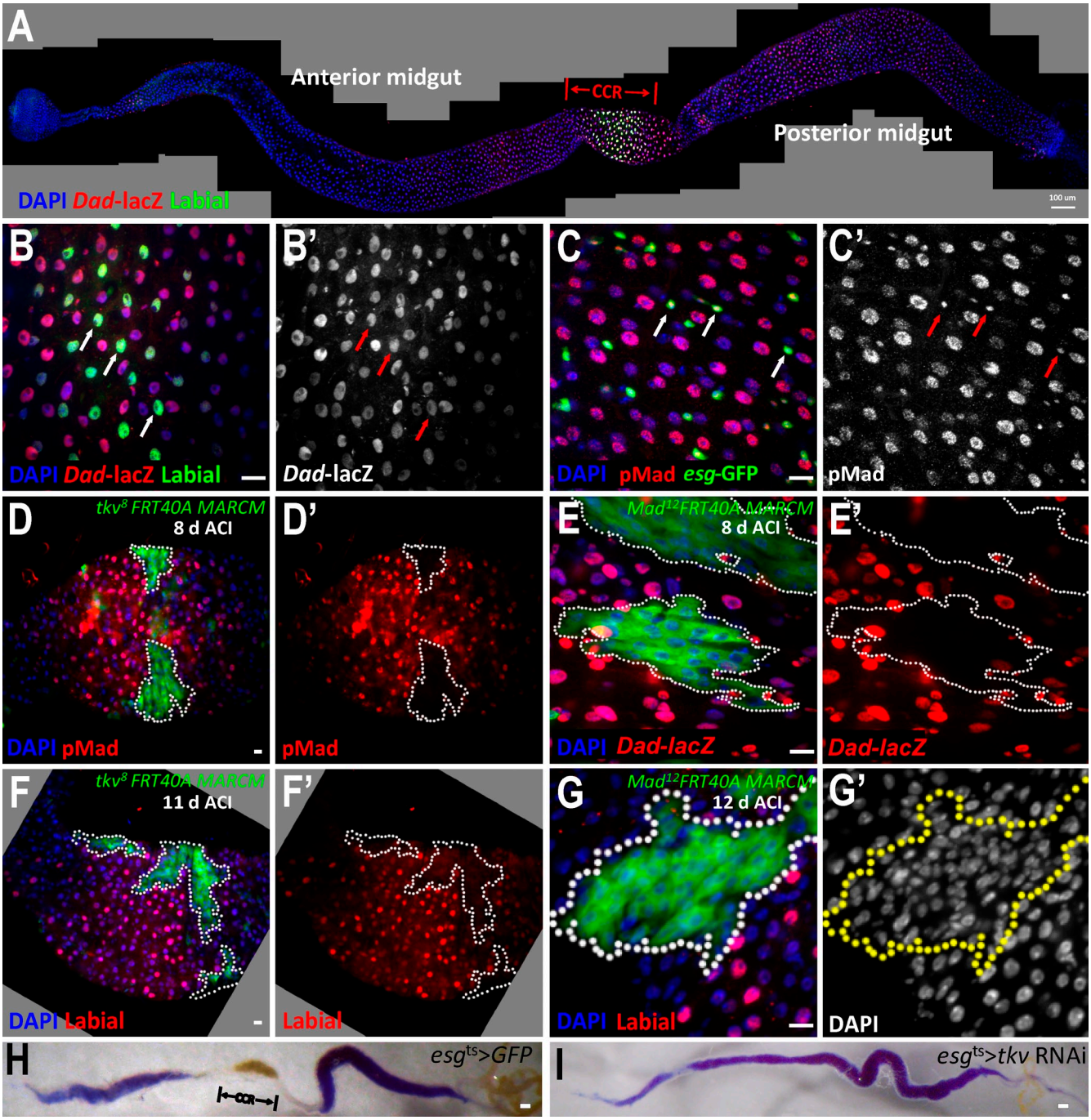

Figure 1. **BMP signaling promotes *Drosophila* copper cell specification.** For all panels, left is anterior, and right is posterior. (A) *Dad-LacZ* expression in the adult midgut. Labial antibody staining marks the copper cell region (CCR). (B and B′) *Dad-lacZ* marks Labial-positive copper cells (arrows). (C and C′) pMad antibody stains *esg-GFP*–positive cells in the CCR (arrows). (D and D′) tkv^8 clones 8 d after clone induction (ACI). pMad staining is absent from tkv^8 clones. (E and E′) Mad^{12} clones 8 d ACI. *Dad-lacZ* staining is absent from Mad^{12} clones. (F and F′) tkv^8 clones 11 d ACI. Labial is absent from tkv^8 clones. (G and G′) Mad^{12} clones 12 d ACI. Nuclei are small, tightly packed, and Labial negative. (H) Bromophenol blue dye staining of the esg^{ts}>*GFP* gut from an animal reared at 30°C for 9 d. The anterior and posterior midgut is blue, pH > 4.6, whereas the CCR is yellow, pH < 3.0. (I) Bromophenol blue dye staining of the esg^{ts}>*tkv* RNAi gut from an animal reared at 30°C for 9 d. CCR loss is indicated by absence of yellow. (D–G) Dashed lines mark clone boundaries. Bars: (A, H, and I) 100 µm; (B–G) 10 µm.

15; Fig. 2, D and D′), a bacteria capable of inducing midgut damage (Basset et al., 2000), and the reactive oxygen species–inducing drug paraquat (Fig. S2, C and C′; Biteau et al., 2008; Choi et al., 2008, 2011; Chatterjee and Ip, 2009; Hochmuth et al., 2011), demonstrating that feeding animals substances that injure the midgut results in up-regulation of BMP signaling.

To determine in which cells of the anterior and posterior midgut BMP signaling is active, we examined pMad and *Dad-lacZ* expression in *esg*-Gal4 UAS-GFP (*esg*>GFP) or *esg*-GFP midguts before (Fig. 2, E–G′; and Fig. S2, D–F′) and immediately after 24 h treatment with bleomycin (Fig. 2, H–J′; and Fig. S2, G–I′). As expected, in the CCR, pMad and *Dad-lacZ*

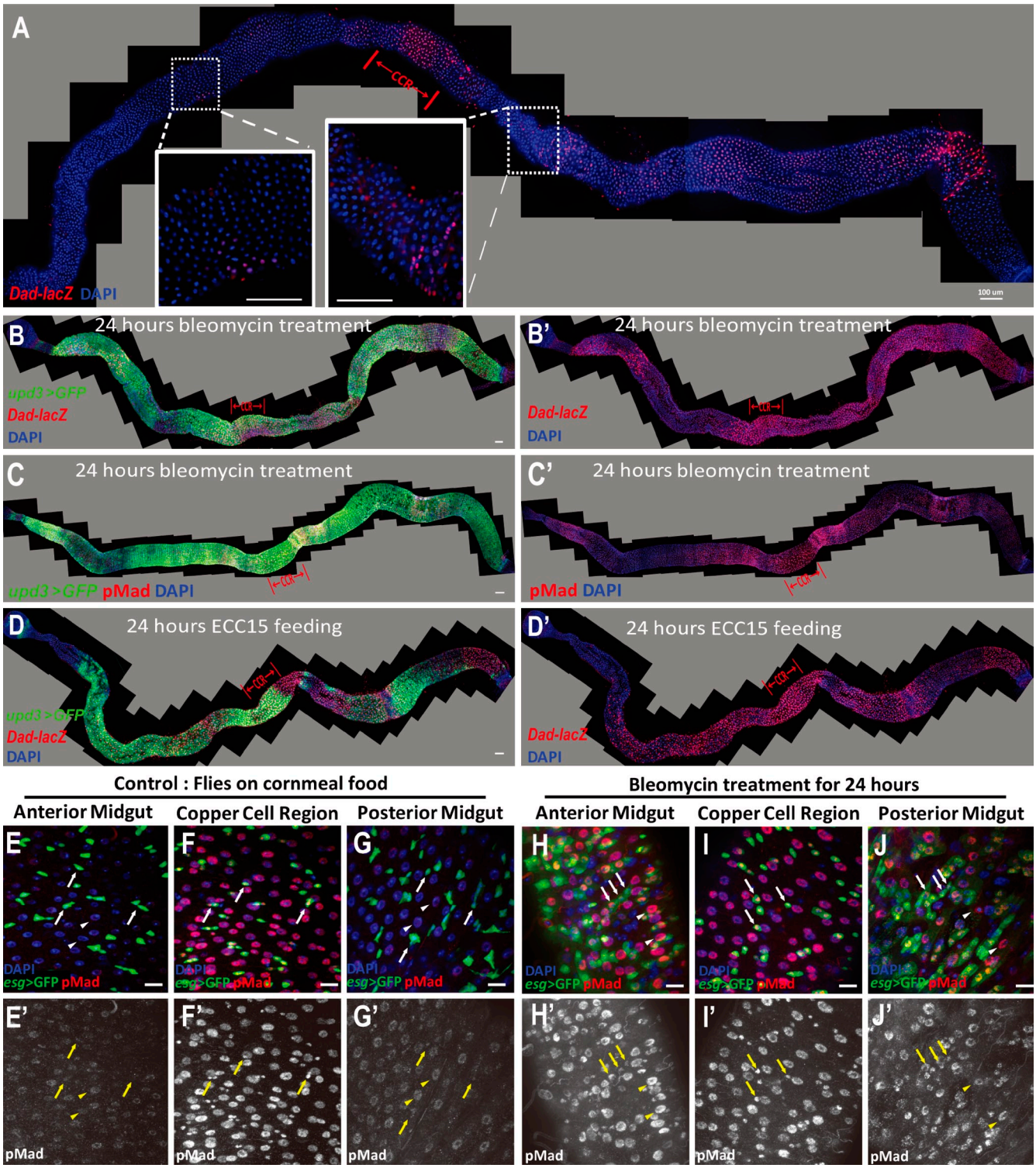

Figure 2. **Injury up-regulates BMP signaling in the midgut.** (A) *Dad-lacZ*–positive cells are present in the anterior and posterior midgut (also see Fig. 1 A). Insets represent close-up views of *Dad-lacZ* in selected regions. (B–C′) *Dad-lacZ* (B and B′), *upd3-Gal4* (B and C), and pMad (C and C′) staining are broadly detectable after 24 h treatment with bleomycin. (D and D′) *Dad-lacZ* and *upd3-Gal4* are broadly detectable after 24 h exposure to *ECC15*. (E–G′) pMad staining from animals reared on a bleomycin-free diet. (H–J′) pMad staining from animals fed bleomycin for 24 h. (E–J′) Arrows show *esg*-GFP–positive cells. Arrowheads show ECs. Bars: (A–D) 100 µm; (E–J) 10 µm.

were expressed in all cells (Fig. 2, F, F′, I, and I′; and Fig. S2, E, E′, H, and H′). In contrast, before bleomycin treatment, the anterior and posterior midgut showed weak pMad and *Dad-lacZ* expression in ECs and much weaker staining in ISCs and EBs (*esg*>GFP- and *esg*-GFP–positive cells; Fig. 2, E, E′, G, and G′; and Fig. S2, D, D′, F, and F′). In the anterior and posterior midguts from animals fed bleomycin, pMad and *Dad-lacZ* expression became intensively elevated in all progenitor cells

(*esg*>GFP- and *esg*-GFP–positive cells) and most ECs (Fig. 2, H, H′, J, and J′; and Fig. S2, G, G′, I, and I′), demonstrating that midgut injury up-regulates BMP signaling in ECs and intestinal progenitors.

BMP signaling negatively regulates midgut homeostasis

Injury to the midgut results in activation of the JNK, JAK-STAT, Yki, EGFR, Pvr (PDGF and VEGF receptor related), and Wnt signaling pathways (Lucchetta and Ohlstein, 2012). These signaling pathways act as part of a positive feedback loop that increases ISC proliferation and daughter differentiation so as to produce new daughters that replace cells lost as a result of injury. Because midgut injury also results in increased BMP signaling, we wondered whether BMP signaling acts in concert with these pathways to promote ISC proliferation and daughter differentiation. Conversely, we considered that BMP signaling acts as part of a negative feedback loop to antagonize ISC activity after injury.

To distinguish between these two possibilities, WT and mutant BMP signaling clones were generated and analyzed in the female posterior midgut. If BMP signaling acts as part of a positive feedback loop, the mean number of cells in mutant ISC clones over time should be less than that of age-matched WT clones. Alternatively, if BMP signaling acts as part of a negative feedback loop, the mean number of cells in mutant ISC clones over time should be greater than that of age-matched WT clones. pMad and *Dad-lacZ* stainings were absent from tkv^{8} and Mad^{12} clones in the anterior and posterior midgut (Fig. S3, A–D′), demonstrating that the mutants we used efficiently block BMP signaling. 8 d after clone induction (ACI), the number of cells in tkv^{8}, tkv^{4}, and Mad^{12} clones was significantly higher than in WT clones (Fig. 3, A–B′ and E), demonstrating that BMP signaling acts as part of a negative feedback loop to restrict the number of cells in a clone.

Because BMP signaling is up-regulated in response to injury, we hypothesized that BMP signaling mutant clones contained more cells because they were located in a region exposed to local injury during the course of the experiment. We next asked whether widespread injury caused by bleomycin would lead to further increases in the number of cells in mutant clones over an 8-d time course. We induced WT and mutant clones as before, injured the gut by feeding flies bleomycin for 24 h between 4 and 5 d ACI, and determined the number of cells per clone 3 d later (8 d ACI). As expected, the number of cells per WT clone increased; however, mutant clones (Fig. 3, D–E) had more cells than both WT clones (Fig. 3, C, C′, and E) and mutant clones before injury (Fig. 3, B, B′, and E).

We next used various cell markers to determine whether ISC daughter fate was affected in mutant clones. By 5 d ACI, WT clones typically contain one Dl-positive stem cell and at least one EC (Fig. 3 F). At 5 d ACI, tkv^{8} clones contained a stem cell (Dl antibody), enteroendocrine cells (Prospero antibody), and ECs (polyploid nuclei; Fig. 3 G), and Mad^{12} clones contained cells positive for the EC marker Pdm-1 (Fig. 3 H; Lee et al., 2009), suggesting that BMP signaling is not required for midgut epithelial cell differentiation. tkv^{8} and Mad^{12} clones also occasionally contained TUNEL-positive cells (Fig. 3 I and Fig. S3 E), suggesting that BMP signaling is not required for apoptosis.

Because BMP signaling reporters can be detected after injury in ISCs and ECs, we considered two possibilities to explain in which cell type BMP signaling acts to regulate the number of cells per ISC clone: (1) BMP signaling is autonomously required in ISCs to limit ISC activity, and (2) BMP signaling in ECs regulates the production of secreted factors that then nonautonomously regulate ISC activity. To determine between these two possibilities, we used cell-specific Gal4 drivers to express *tkv* and *Mad* RNAi and examined the effect on $PH3^{+}$ number in the posterior midgut. RNAi knockdown of *Mad* or *tkv* in ISCs and EBs using esg^{ts} (Fig. 3, J–L) or the ISC driver *Dl*-Gal4 (Fig. 3 L and Fig. S3, F–F‴) at 30°C for 8 d led to a dramatic increase in PH3-positive cell number in the posterior midgut as compared with sibling controls (Fig. 3 L), demonstrating that BMP signaling acts autonomously in ISCs to regulate midgut homeostasis. Strikingly, although we found that RNAi knockdown of *Mad* or *tkv* in ECs by $Myo1A^{ts}$ (Jiang et al., 2009) decreased *Dad*-LacZ and pMad expression in ECs after 8 d (Fig. S3, G–H′ and J–K′), it had no effect on $PH3^{+}$ number (Fig. 3 L and Fig. S3 I), further demonstrating that BMP signaling acts autonomously in ISCs to regulate their proliferation rate.

BMP signaling activation antagonizes midgut response to injury

Loss of BMP signaling results in an exaggerated response of the midgut to injury. We next asked whether increased BMP signaling could attenuate the response of the midgut to damage. To increase BMP signaling, we made clones of Dad^{212} (Ogiso et al., 2011), a physiological target of and negative regulator of the BMP signaling pathway, or MARCM clones expressing an activated form of *tkv* (tkv^{CA}; Adachi-Yamada et al., 1999). In weak pMad staining regions, relatively high pMad staining was present in Dad^{212} clones (Fig. S4, A and A′) and in clones (Fig. S4, B and B′) expressing UAS-tkv^{CA} (Fig. S4, B and B′), demonstrating that loss of Dad or expression of activated *Tkv* results in an autonomous increase in BMP signaling.

3 d ACI, flies were divided into two groups: one group of flies was fed bleomycin for 24 h and then transferred to control food every 24 h for the remainder of the experiment. The remaining group of flies was fed control food for 24 h and then transferred to control food every 24 h for the remainder of the experiment. At 4, 5, and 6 d ACI, midguts were analyzed from each cohort to determine the number of cells per clone (Fig. S4 C).

The mean number of cells in WT clones (Fig. 4 Q, blue dots) from animals reared on control food, increased from 4 d ACI to 6 d ACI (Fig. 4, A and Q). The mean number of cells in $punt^{135}$ (type II BMP receptor mutant) clones (Fig. 4 Q, red dots) also increased from 4 d ACI to 6 d ACI (Fig. 4, E and Q) and, as expected, contained more cells that WT clones. In contrast, the mean number of cells in Dad^{212} (Fig. 4 Q, green dots) or UAS-tkv^{CA} (Fig. 4 Q, purple dots) clones had fewer cells than WT clones from 4 d to 6 d ACI (Fig. 4, I, M, and Q).

After 24-h bleomycin treatment, the mean cell number per $punt^{135}$ clone (Fig. 4, F–H and R, red dots) was larger than the mean cell number per WT clone (Fig. 4, B–D and R, blue dots) 24, 48, and 72 h after bleomycin treatment. Although mean cell number increased in Dad^{212} or UAS-tkv^{CA} clones 24 h after

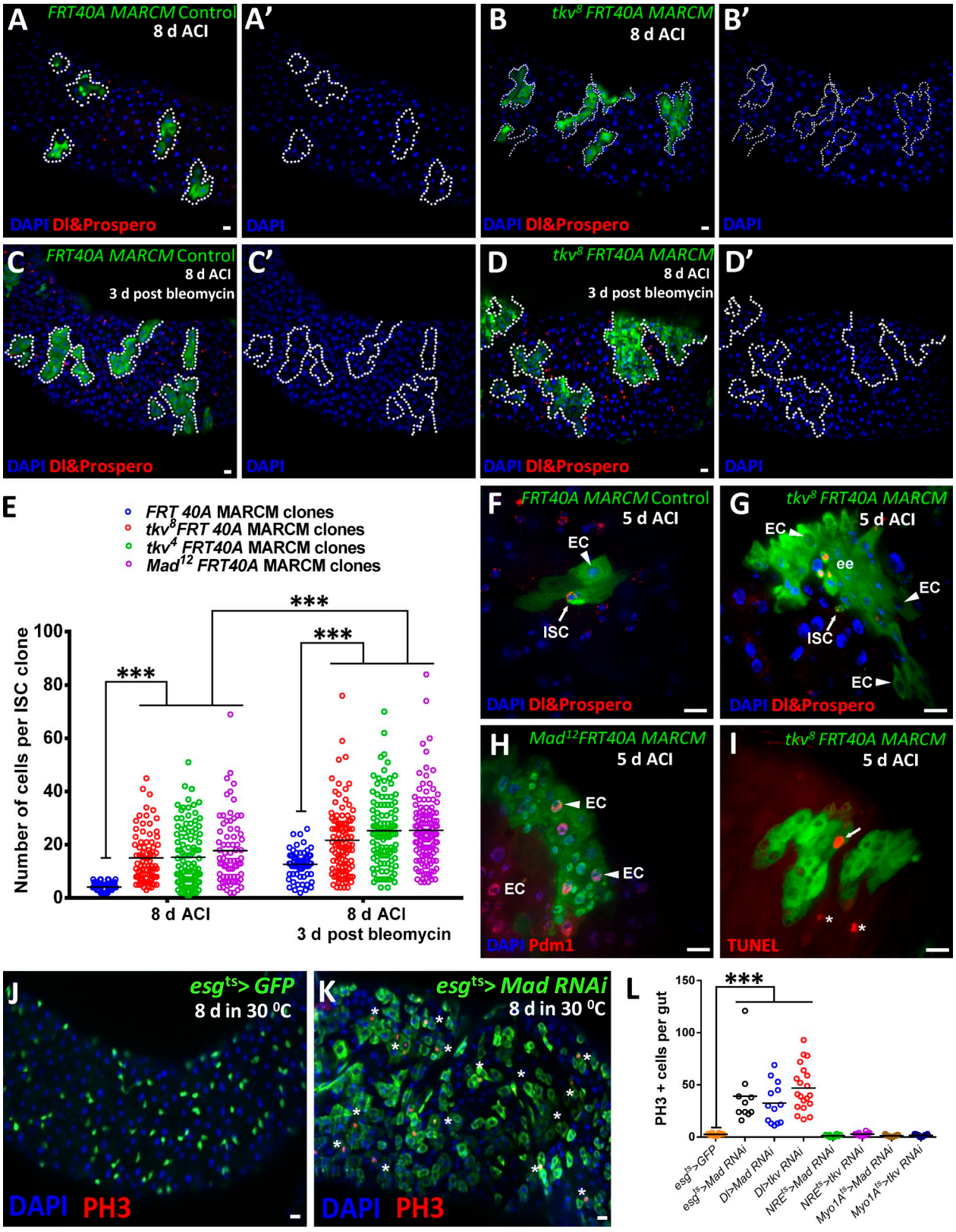

Figure 3. **BMP signaling negatively regulates midgut homeostasis.** (A and B) Control and *tkv*^{8} clones 8 d after clone induction (ACI), in the posterior midgut. (C and D) WT and *tkv*^{8} clones 8 d ACI, in the posterior midgut from animals fed bleomycin for 24 h between 4 and 5 d ACI. (E) Quantification of ISC clone size (number of cells per ISC clone) in posterior midguts of indicated genotypes. The data shown are from a single representative experiment out of four repeats. Each dot corresponds to one ISC clone. 8 d ACI, *n* = 82 (*40A*, five guts), 82 (*tkv*^{8}, six guts), 108 (*tkv*^{4}, seven guts), and 74 (*Mad*^{12}, six guts). 8 d ACI, 3 d after bleomycin, *n* = 67 (*40A*, four guts), 111 (*tkv*^{8}, six guts), 113 (*tkv*^{4}, eight guts), and 127 (*Mad*^{12}, five guts). The black bars indicate mean value. ***, P < 0.0001, by one-way ANOVA test. (F) At 5 d ACI, a control MARCM clone contains one stem cell (Dl staining, arrow) and at least one EC (arrowhead). (G) A *tkv*^{8} clone contains a stem cell (Dl staining, arrow), enteroendocrine (ee) cells (Prospero staining), and ECs (arrowheads). (H) *Mad*^{12}

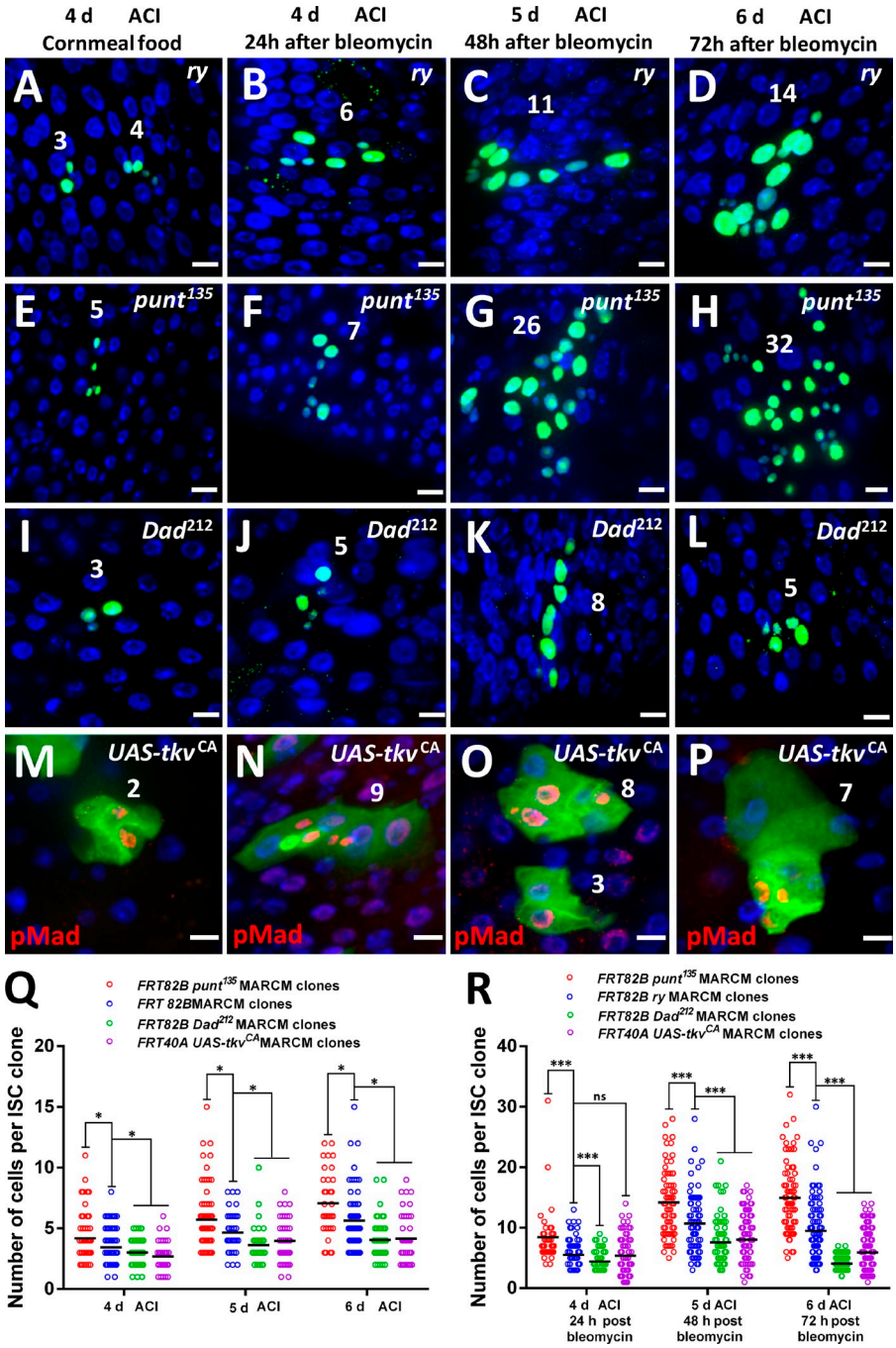

Figure 4. **BMP signaling antagonizes injury-induced ISC proliferation.** (A–P) Representative examples of WT, BMP mutant, and constitutive active *tkv* (*tkv*^{CA}) clones from animals reared on food with or without bleomycin. Green marks cells within a clone. Cell number per clone is given in white. (B–D) WT clones respond to injury by expanding cell number. (F–H) *punt*^{135} clones respond to injury by rapidly expanding cell number. *punt*^{135} clones reach a larger clone size (G and H) than WT. (J–L) *Dad*^{212} clones respond to the injury by increasing cell number (J and K). (J and K) *Dad*^{212} clones reach a smaller clone size than WT clones 24 h after injury. (L) The difference is most prominent 72 h after injury. (M–P) *tkv*^{CA} ectopic expression clones respond to the injury by increasing cell number (N–P). (O) *tkv*^{CA} clones reach a smaller clone size than WT clones 48 h after injury. (P) The difference is most prominent 72 h after injury. pMad staining reveals activation of BMP signaling in *tkv*^{CA} clones. (Q) Quantification of clone sizes in flies fed control food. This experiment was completed once. Each dot corresponds to one ISC clone. At 4 d ACI, *n* = 58 (*punt*^{135}, eight guts), 93 (*82B*, eight guts), 94 (*Dad*^{212}, six guts), and 36 (*tkv*^{CA}, four guts). At 5 d ACI, *n* = 79 (*punt*^{135}, nine guts), 39 (*82B*, eight guts), 43 (*Dad*^{212}, four guts), and 40 (*tkv*^{CA}, four guts). At 6 d ACI, *n* = 33 (*punt*^{135}, seven guts), 80 (*82B*, nine guts), 55 (*Dad*^{212}, five guts), and 42 (*tkv*^{CA}, five guts). The black bars indicate mean values. *, P < 0.01, by one-way ANOVA test. (R) Quantification of clone size after induction of injury by bleomycin. This experiment was completed once. Each dot corresponds to one ISC clone. At 4 d ACI, 24 h after bleomycin, *n* = 45 (*punt*^{135}, seven guts), 79 (*82B*, 13 guts), 76 (*Dad*^{212}, seven guts), and 132 (*tkv*^{CA}, 10 guts). At 5 d ACI, 48 h after bleomycin, *n* = 67 (*punt*^{135}, eight guts), 80 (*82B*, eight guts), 82 (*Dad*^{212}, nine guts), and 121 (*tkv*^{CA}, nine guts). At 6 d ACI, 72 h after bleomycin, *n* = 71 (*punt*^{135}, four guts), 96 (*82B*, seven guts), 162 (*Dad*^{212}, eight guts), and 137 (*tkv*^{CA}, 11 guts). The black bars indicate mean values. ***, P < 0.0001, by one-way ANOVA test. Bars, 10 µm.

bleomycin, *Dad*^{212} clones had fewer cells than WT clones (Fig. 4, J–L and R, green dots) 24, 48, and 72 h after bleomycin treatment. UAS-*tkv*^{CA} clones also had fewer cells than WT clones (Fig. 4, O, P, and R, purple dots) 48 and 72 h after bleomycin treatment. Together, these gain-of-function experiments suggest that activation of the BMP signaling pathway antagonizes the response of ISCs to injury.

BMP signaling regulates both ISC number and the rate of ISC division

Increased cell number in BMP signaling mutant ISC clones could be caused by an increase in stem cell number per clone and/or an increased rate of stem cell division. The only known cell to divide in the midgut is the ISC. Therefore, a PH3-positive cell should indicate an ISC in mitosis. However, because mitosis

clones contain Pdm1-positive ECs (arrowheads). (I) Cells undergoing programmed cell death (TUNEL positive) in a *tkv*^{8} clone (arrow) and in surrounding WT tissue (asterisks). (J and K) Loss of *Mad* in progenitor cells results in increased PH3^{+} cells (asterisks) in the posterior midgut. *Mad* RNAi was driven by *esg-Gal4*^{ts} at 30°C for 8 d. (L) PH3^{+} cell number in the posterior midgut from indicated genotypes. *Mad* RNAi and *tkv* RNAi were driven at 30°C for 8 d. The data shown are from a single representative experiment out of three repeats. Each dot corresponds to one gut. The number of guts from left to right are as follows: 10, 10, 13, 20, 10, 12, 11, and 11. ***, P < 0.0001, by one-way ANOVA test. Bars, 10 µm.

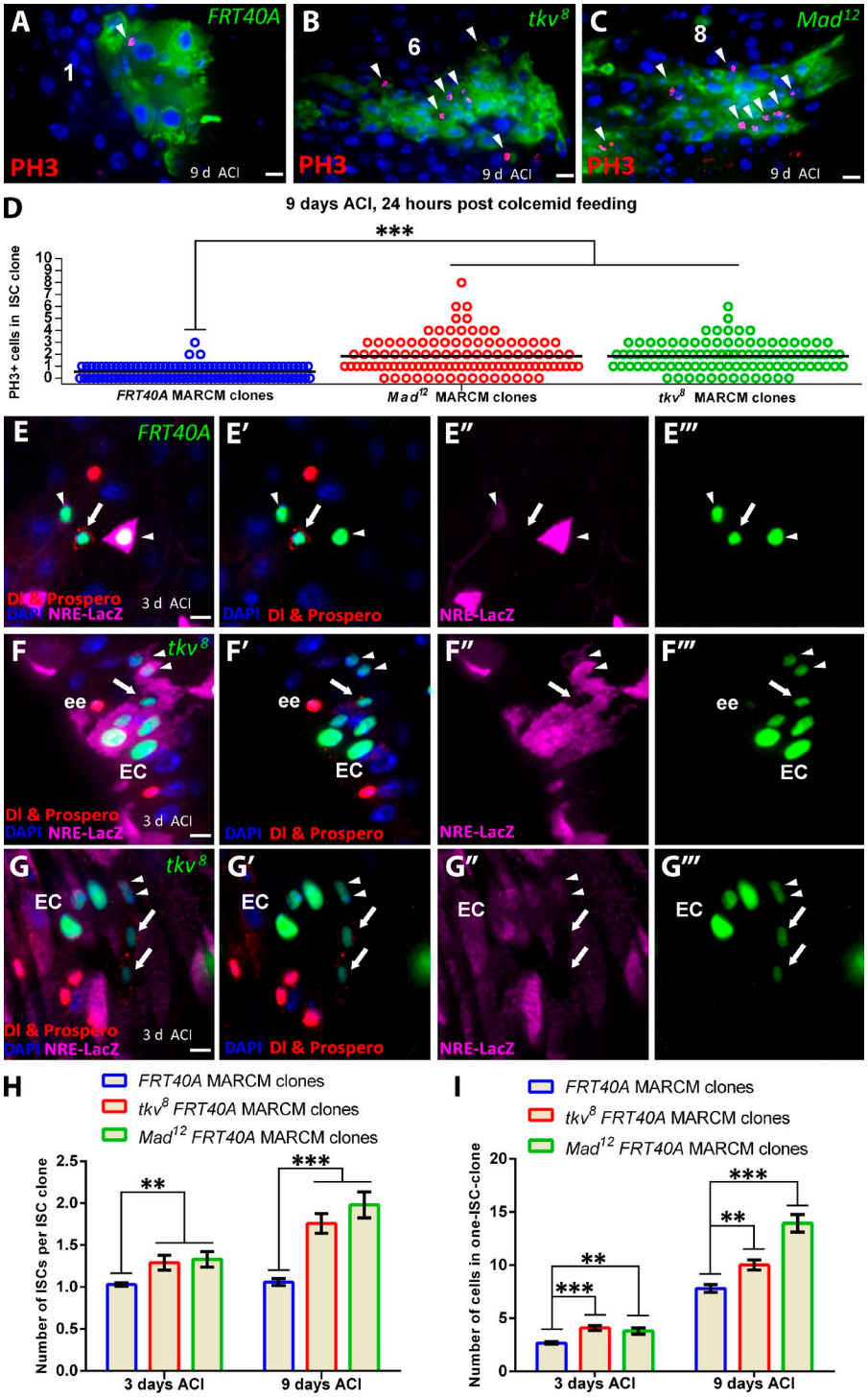

Figure 5. **BMP signaling regulates stem cell number and rate of stem cell division.** (A–C) 24 h after colcemid feeding, one PH3+ cell is present in a WT clone (A), 9 d after clone induction (ACI). Six PH3+ cells are present in a *tkv*^{8} MARCM clone (B), and eight PH3+ cells are present in a *Mad*^{12} clone (C), 9 d ACI. PH3+ cell number per clone is given in white. Arrowheads show PH3+ cells. (D) Quantification of PH3+ cells in WT, *tkv*^{8}, and *Mad*^{12} clones 9 d ACI, 24 h after colcemid. This experiment was completed once. Each dot corresponds to one ISC clone. *n* = 102 (*40A*), 108 (*Mad*^{12}), and 103 (*tkv*^{8}). The black bars indicate mean values. (E–E‴) A WT clone with one ISC, 3 d ACI. (F–G‴) *tkv*^{8} clones at 3 d ACI with one (F) or two ISCs (G). Arrows show ISCs; arrowheads show EBs. (H) Quantification of stem cell number in WT, *tkv*^{8}, and *Mad*^{12} clones 3 d ACI or 9 d ACI. At 3 d ACI, mean stem cell number per clone was 1.03:1.29:1.33 (WT/*tkv*^{8}/*Mad*^{12}). At 9 d ACI, mean stem cell number per clone was 1.06:1.76:1.98 (WT/*tkv*^{8}/*Mad*^{12}). (I) Quantification of clone size in WT, *tkv*^{8}, and *Mad*^{12} clones that contain one ISC. One-stem-cell *tkv*^{8} and *Mad*^{12} clones are larger than one-stem-cell WT at 3 d ACI and 9 d ACI. Mean number of cells per one-stem-cell clone at 3 d ACI was 2.68:4.06:3.79 (WT/*tkv*^{8}/*Mad*^{12}), and at 9 d ACI, it was 7.81:10.03:13.94 (WT/*tkv*^{8}/*Mad*^{12}). Data are represented as means ± SEM. **, P < 0.001; ***, P < 0.0001, by one-way ANOVA test. Bars, 10 µm.

represents a small window of the cell cycle, it is difficult to identify clones that contain a PH3+ cell. We therefore used colcemid, a microtubule-depolymerizing drug that disrupts the mitotic spindle, thereby arresting dividing cells in metaphase. ISCs that divide during the period of colcemid feeding will remain PH3+, allowing one to capture a broad window of ISC divisions. We generated WT, *tkv*^{8}, and *Mad*^{12} clones, fed animals colcemid between 8 and 9 d ACI, and counted PH3+ cell number per clone 9 d ACI (Fig. 5, A–C). WT clones contained on average 0.53 PH3+ cells per clone, whereas *tkv*^{8} and *Mad*^{12} clones contained on average 1.83 and 1.84 PH3+ cells per clone, respectively (Fig. 5 D), suggesting that mutant clones contain more than one ISC.

In further support of our observation that mutant clones contained more than one ISC, we generated WT, *tkv*^{8}, and *Mad*^{12} clones and counted the number of ISCs and the total number of cells in each clone. At 3 d ACI, 67 of 69 WT clones contained one stem cell (Fig. 5, E–E‴ and H), whereas 11 of 45 *tkv*^{8} clones (Fig. 5, F–H) and 12 of 40 *Mad*^{12} already contained more than one stem cell (Fig. 5 H). At 9 d ACI, 30 of 62 *tkv*^{8} and 26

of 42 *Mad*^{12} clones contained more than one stem cell (Fig. 5 H), whereas 32 of 34 WT clones still contained one stem cell (Fig. 5 H), demonstrating that loss of BMP signaling results in a gradual increase in ISC number over time.

To determine whether ISCs divide more often in mutant clones than in WT clones, we compared the total number of cells per clone from one-stem-cell WT, one-stem-cell *tkv*^{8}, and one-stem-cell *Mad*^{12} clones. One-stem-cell *tkv*^{8} clones (n = 34, 3 d ACI; or n = 32, 9 d ACI) and one-stem-cell *Mad*^{12} clones (n = 28, 3 d ACI; or n = 16, 9 d ACI) contained more cells than WT clones (n = 67, 3 d ACI; or n = 32, 9 d ACI; Fig. 5 I), indicating that BMP mutant ISCs divide more often than WT ISCs. Thus, our data suggest that mutant clone growth results from increases in ISC proliferation and ISC number.

Loss of BMP signaling–induced ISC proliferation requires EGFR signaling

JAK-STAT and EGFR signaling are activated in ISCs after tissue injury or bacterial infection (Buchon et al., 2009; Jiang et al., 2009, 2011; Buchon et al., 2010). Given that BMP signaling antagonizes injury-induced ISC proliferation, we investigated whether each signaling pathway was required to be activated for BMP signaling to exert its effect.

To block JAK-STAT signaling, we made MARCM clones expressing an RNAi against *Stat92E*. Consistent with studies that JAK-STAT signaling is required for EC differentiation (Jiang et al., 2009; Beebe et al., 2010), expression of *Stat92E* RNAi in MARCM clones resulted in clones lacking ECs (Fig. 6, A and D). At 8 d ACI, *Stat92E RNAi* (Fig. 6 A) clones were significantly smaller than BMP signaling mutant clones (Fig. 6, B and J). However, although ectopic expression of *Stat92E RNAi* in *Mad*^{12} ISC MARCM clones (Fig. 6 C) blocked EC differentiation, it had no effect on clone cell number (Fig. 6 J), suggesting that increases in cell number seen with BMP signaling mutant clones do not require JAK-STAT signaling. Because JAK-STAT signaling is sufficient but not required for ISC proliferation (Jiang et al., 2009; Beebe et al., 2010), we next examined the effect of bleomycin treatment, a potent inducer of JAK-STAT signaling (Jiang et al., 2009; Beebe et al., 2010), on the growth of BMP signaling and JAK-STAT signaling double mutant clones. At 8 d ACI, 3 d after bleomycin, both *Mad*^{12} and *Mad*^{12}; UAS-*Stat92E RNAi* clones (Fig. 6, E, F, and J) were larger than *Stat92E RNAi* clones (Fig. 6, D and J). These epitasis experiments demonstrate that JAK-STAT signaling is not required for loss of BMP signaling–induced ISC proliferation.

To block EGFR signaling, we made clones expressing UAS-*Ras*^{DN}. Consistent with previous studies (Biteau and Jasper, 2011; Jiang et al., 2011), we found that ectopic expression of *Ras*^{N17} (*Ras*^{DN}) dramatically inhibited the clone growth (Fig. 6 G). Expression of *Ras*^{DN} in *tkv*^{8} or *Mad*^{12} clones also dramatically decreased BMP signaling mutant clone sizes (Fig. 6, H, I, and J). Similar results were obtained for both *tkv*^{8}; UAS-*Ras*^{DN} and *Mad*^{12}; UAS-*Ras*^{DN} clones after bleomycin treatment (Fig. 6 J). Thus, active EGFR signaling is required for loss of BMP signaling–induced ISC proliferation.

dpp expressed in vm regulates midgut homeostasis

In *Drosophila*, three ligands, *dpp*, *screw*, and *glass bottom boat*, are known to activate the BMP signaling pathway (Wharton and Derynck, 2009). Real-time quantitative PCR (RT-qPCR) from total midgut RNA revealed that *dpp* is expressed in the midgut and is up-regulated along with *Dad* (Tsuneizumi et al., 1997), a target of BMP signaling, and *upd3*, a marker of damaged cells (Jiang et al., 2009), by bleomycin treatment, suggesting that it might promote injury-induced midgut BMP signaling (Fig. 7 A). Recently, by in situ hybridization analysis and lacZ staining of a *P* element enhancer trap in the *dpp* gene (*dpp*^{10638}; Jiang and Struhl, 1995), Li et al. (2013) reported that *dpp* is expressed in the trachea of the midgut, where it acts to regulate EC viability and midgut homeostasis. Because *dpp* levels increase after injury (Fig. 7 A), we examined the expression of lacZ in *dpp*^{10638} flies fed paraquat. Consistent with Li et al. (2013), we found that lacZ was strongly expressed in midgut trachea. However, as a new finding, lacZ was detected in circular muscle (Fig. S5, A and A′). In addition, we were able to identify by in situ hybridization the expression of *dpp* in circular muscle (Fig. S5 B), suggesting that midgut vm might be a source of functionally relevant *dpp*.

To gain further insight into the relevant midgut expression pattern of *dpp*, we screened a collection of 12 putative *dpp* enhancer-Gal4 lines available from the Bloomington Stock Center (FlyBase; Pfeiffer et al., 2008). Two of these Gal4 lines containing ∼1-kb overlapping DNA sequences (Fig. S5 C) drove UAS-GFP expression in midgut circular muscle (Fig. 7 B), whereas the remaining 10 Gal4 lines failed to drive expression (not depicted). Of the two lines, one has a stronger expression pattern, which we refer to as *dpp*-Gal4^{gut} (*dpp*^{gut}). Both Gal4 lines drive expression of UAS-GFP in terminal filament and cap cells in the *Drosophila* germarium (Fig. S5 D). The terminal filament and cap cells are the proposed cellular source of Dpp that maintains female germline stem cells (Xie and Spradling, 1998; Guo and Wang, 2009), suggesting that these Gal4 lines are driven by *dpp* enhancer sequences. Several other pieces of data indicate that *dpp*-Gal4^{gut} UAS-GFP (*dpp*^{gut}>GFP) represents part of the endogenous midgut *dpp* expression pattern: *dpp*^{gut}>GFP expression is strong in circular muscle of the CCR yet highly variable in the circular muscle of the anterior and posterior midgut (Fig. 7 B). *dpp*^{gut}>GFP expression becomes broadly expanded in circular muscle along the midgut after 24 h of bleomycin treatment (Fig. 7 C), consistent with increases in *dpp* RNA levels seen after bleomycin treatment (Fig. 7 A).

To identify which cellular source of Dpp is functionally relevant, we used cell-specific drivers and UAS-*dpp* RNAi to knockdown *dpp* expression and examined the effect on Labial and pMad expression. Expression of *dpp-RNAi* by the temperature-inducible vm-specific driver *how*-Gal4 UAS-GFP; *tub-Gal80*^{ts} for 8 d at the permissive temperature eliminated pMad staining in the CCR and anterior midgut (Fig. S5 E). However, in contrast to claims that *how*-Gal4 is muscle specific in the adult (Jiang et al., 2009, 2011; Li et al., 2013), we found that *how-Gal4* UAS-GFP is expressed in both vm and trachea (Fig. S5 F), an expression pattern identical to that reported in the larval midgut

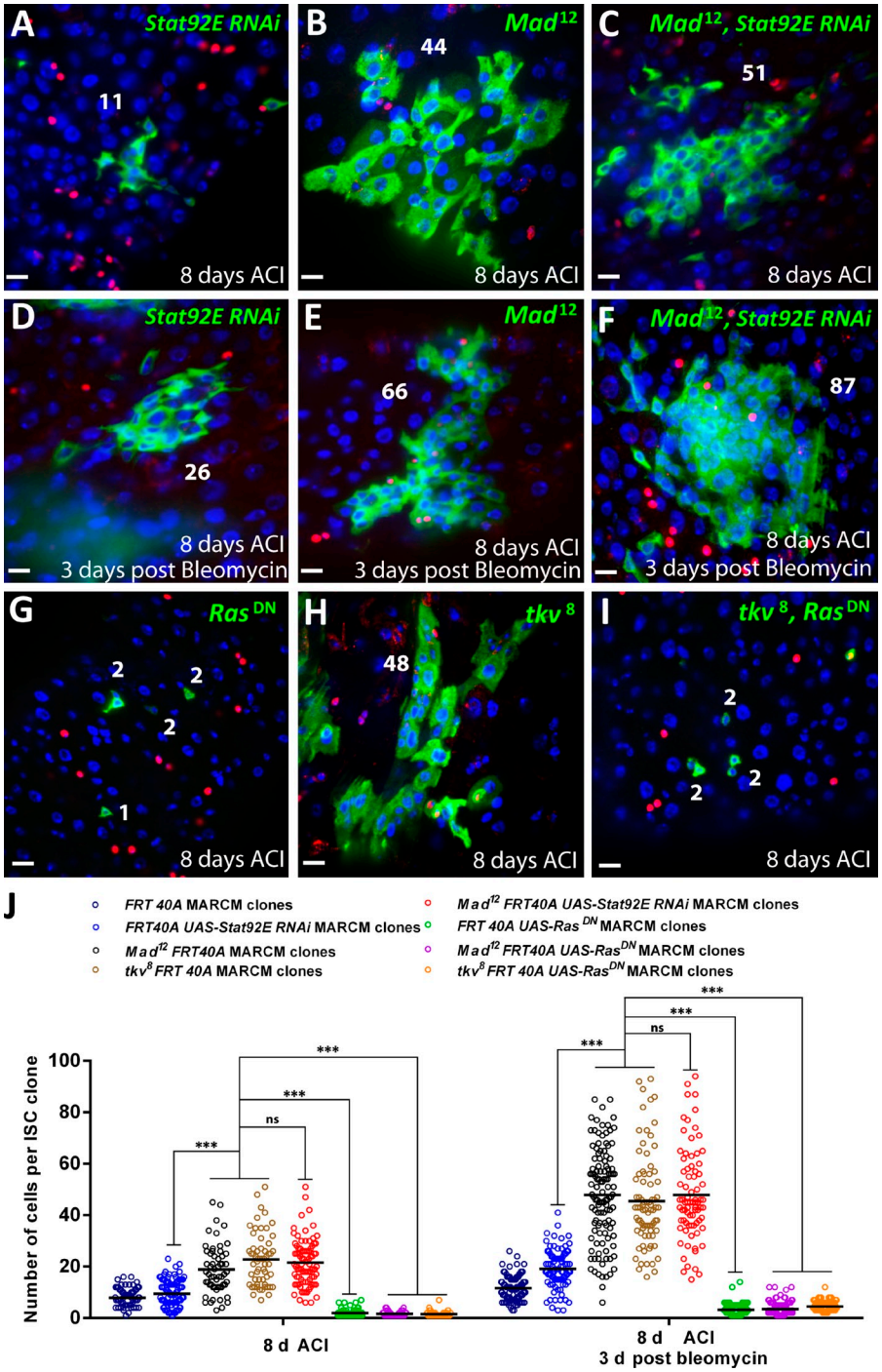

Figure 6. **Loss of BMP signaling–induced ISC proliferation requires EGFR signaling but not JAK-STAT signaling.** (A–I) Green (GFP) marks cells within a clone. Red shows Dl and Prospero staining. The number of cells per clone is indicated next to each clone. (A–C) *UAS-Stat92E RNAi* clone (A), Mad^{12} clone (B), and Mad^{12}, *UAS-Stat92E RNAi* clone (C) 8 d after clone induction (ACI) in the posterior midgut reared on a bleomycin-free diet. (D–F) *UAS-Stat92E RNAi* clone (D), Mad^{12} clone (E), and Mad^{12}; *UAS-Stat92E RNAi* clone (F) 8 d ACI, in the posterior midgut from animals reared on bleomycin for 24 h between 4 and 5 d ACI. (G–I) *UAS-*Ras^{DN} clone (G), tkv^{8} clone (H), and tkv^{8}; *UAS-*Ras^{DN} clone (I) 8 d ACI in the posterior midgut reared on a bleomycin-free diet. (J) Quantification of clone sizes in the posterior midgut from the indicated genotypes. This experiment was completed once. Each dot corresponds to one ISC clone. At 8 d ACI, $n = 72$ (*40A*, four guts), 99 (*Stat92E RNAi*, five guts), 57 (Mad^{12}, four guts), 59 (tkv^{8}, four guts), 85 (Mad^{12}; *UAS-Stat92E RNAi*, four guts), 137 (Ras^{DN}, five guts), 83 (Mad^{12}; *UAS-*Ras^{DN}, four guts), and 88 (tkv^{8}; *UAS-* Ras^{DN}, four guts). At 8 d ACI, 3 d after bleomycin, $n = 105$ (*40A*, five guts), 88 (*Stat92E RNAi*, three guts), 117 (Mad^{12}, four guts), 80 (tkv^{8}, three guts), 79 (Mad^{12}; *UAS-Stat92E RNAi*, four guts), 108 (Ras^{DN}, six guts), 155 (Mad^{12}; *UAS-* Ras^{DN}, six guts), and 126 (tkv^{8}; *UAS-*Ras^{DN}, seven guts). The black bars indicate mean values. ***, $P < 0.0001$, by one-way ANOVA test. Bars, 10 µm.

(Jiang and Edgar, 2009). Given the lack of specific vm expression by *how*-Gal4, we used *dpp*-$Gal4^{gut}$ to express *dpp* RNAi in vm. Expression of *dpp-RNAi* by *dpp*-$Gal4^{gut}$ dramatically decreased pMad and Labial staining in the CCR (Fig. 7, D–E′; and Fig. S5, G and H). In a screen of a collection of Gal4 lines generated by Pfeiffer et al. (2008), we identified another vm driver, *vm*-Gal4 (Fig. S5 I). Expression of *dpp-RNAi* at 30°C for 8 d by *vm*-Gal4 also dramatically decreased pMad (Fig. 7, F and F′) and Labial (Fig. S5 J) staining in the midgut, further demonstrating that Dpp is required in vm to initiate and maintain BMP signaling in the intestine.

By heat shock–inducible flippase induction (See Materials and methods), conversion of *tub*-flippase recognition target (FRT)-Gal80-FRT, *vm-Gal4* to *tub*-FRT, *vm*-Gal4 results in Gal4 expression in circular muscle in a mosaic pattern. We used this convertible *tub*-FRT-Gal80-FRT, *vm*-Gal4 system (referred to as vm^{flp}) to express UAS-GFP and UAS-*dpp* RNAi (vm^{flp}>*dpp* RNAi; Fig. 7 G) in subsets of vm. Only in epithelial regions adjacent to vm^{flp}>*dpp* RNAi-positive circular muscle was pMad staining absent (Fig. 7, H–H″). In contrast to claims by Li et al. (2013), expression of *dpp* RNAi in trachea using *btl*-Gal4 (Fig. S5, K–L′) or *14D03*-Gal4 (Fig. S5 M) had no effect on

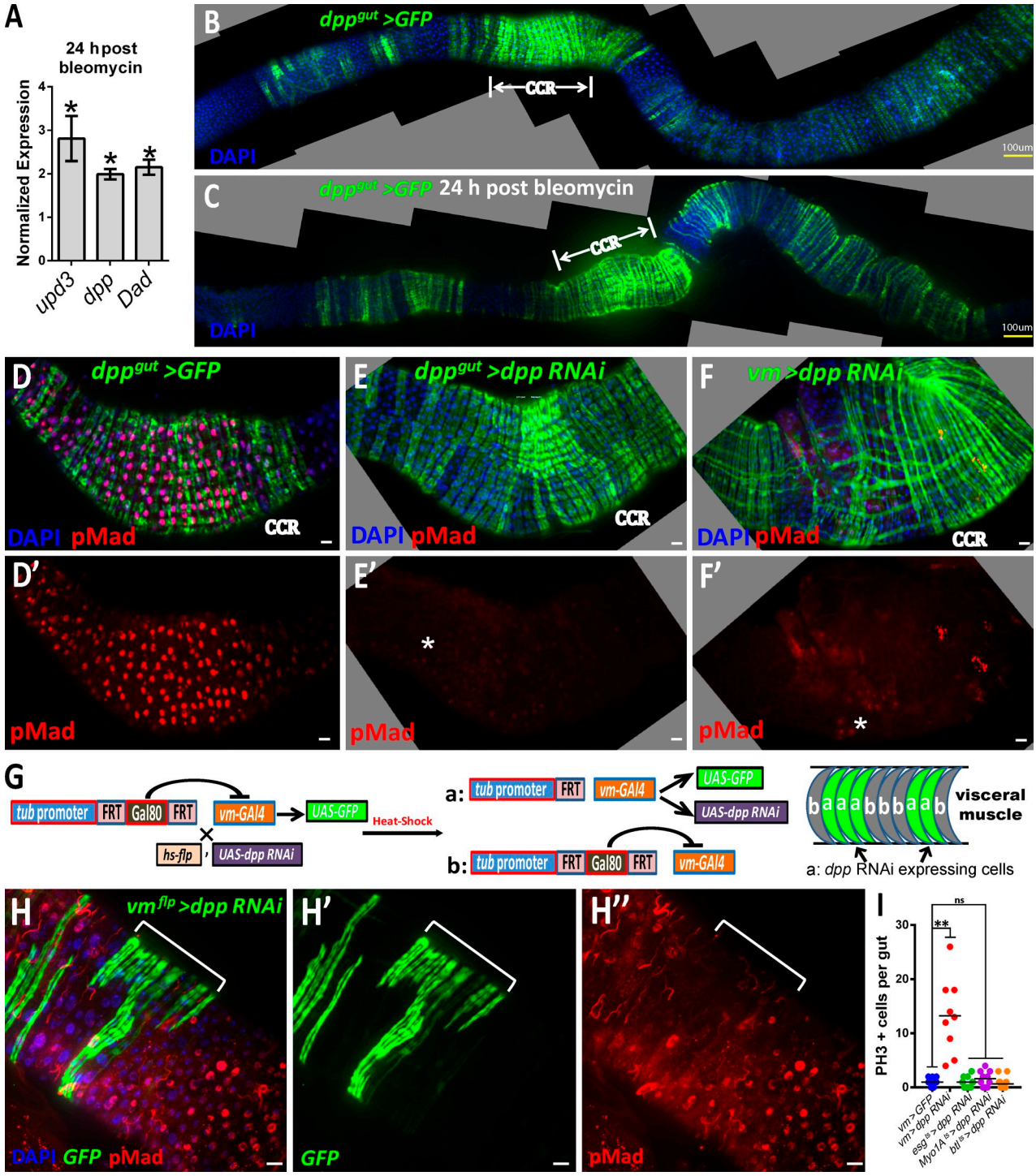

Figure 7. **Dpp is required in vm to regulate midgut homeostasis.** (A) RT-qPCR demonstrates that bleomycin-induced injury increases levels of *upd3*, *dpp*, and *Dad* mRNA in the midgut. Data are represented as means ± SEM. *, $P < 0.01$, by Student's *t* test. (B) *dpp-Gal4^{gut}* is expressed in adult midgut circular muscle. *dpp^{gut}>GFP* (*dpp-Gal4^{gut} UAS-GFP*) expression is strongest in circular muscle associated with the copper cell region (CCR); however, regions of weaker expression are present in anterior and posterior midgut circular muscle. (C) 24 h after treatment with bleomycin, *dpp^{gut}>GFP* becomes strongly expressed in circular muscle throughout most of the midgut. (D and D′) pMad staining in the CCR of *dpp^{gut}>GFP*. (E and E′) Expression of *dpp* RNAi in circular muscle by *dpp-Gal4^{gut}* results in decreased pMad staining in the CCR. (E′) Asterisk indicates weak pMad staining. Picture was taken at the same setting as D. (F and F′) Expression of *dpp* RNAi in midgut vm by *vm-Gal4^{ts}* results in decreased pMad staining in the CCR. (F′) Asterisk indicates weak pMad staining. Picture was taken at the same setting as D. (G) Diagram describing generation of mosaic expression *of dpp* RNAi in vm. (H–H″) 8 d after heat shock and 24 h after bleomycin treatment, GFP and *dpp RNAi* are expressed in a subset of circular muscle bands in the posterior midgut. Note that pMad staining is absent in regions adjacent to GFP-positive vm (brackets). (I) Quantification of PH3$^+$ cells in posterior midguts from the indicated genotypes. *dpp* RNAi was driven at 30°C for 8 d. The data shown are from a single representative experiment out of three repeats. Each dot corresponds to one midgut. The number of guts from left to right are as follows: 10, 9, 11, 10, and 18. **, $P < 0.001$, by one-way ANOVA test. Bars: (B and C) 100 µm; (D–F and H) 10 µm.

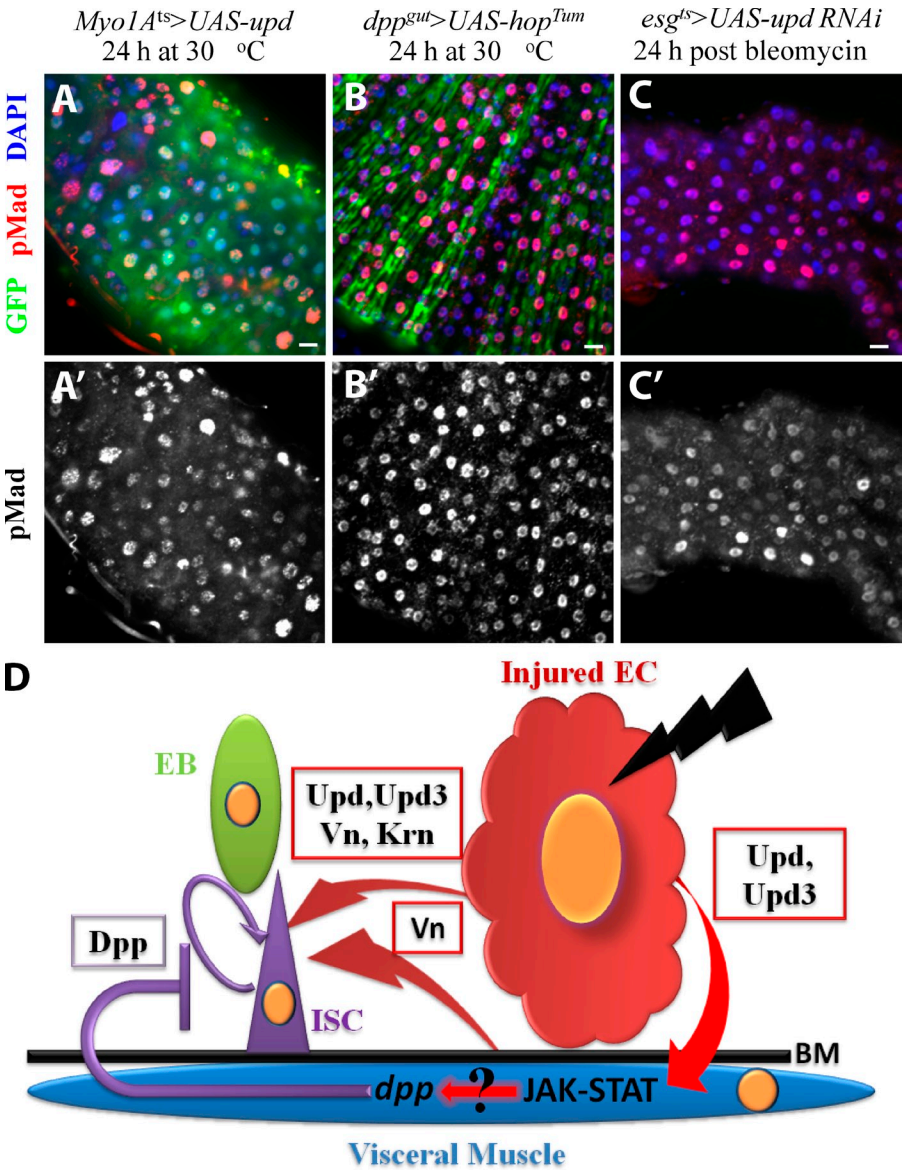

Figure 8. **JAK-STAT signaling can induce BMP signaling in midgut epithelium.** (A and A′) Expression of Upd in ECs with *Myo1A*^{ts}-*Gal4* for 24 h resulted in high levels of pMad staining (A′) in midgut epithelium. (B and B′) Expression of *UAS-hop*^{Tum} in vm with *dpp*^{Gut}-*Gal4* for 24 h induced high levels of pMad staining (B′) in midgut epithelium. (C) ISCs and EBs were ablated by *esg*^{ts}*>UAS-Upd RNAi* for 8 d at 30°C. (C′) After 24-h bleomycin treatment, ECs stain positive for pMad. (D) Model describing how injury-induced BMP signaling regulates midgut homeostasis. EB, enteroblast; BM, basal membrane; Vn, Vein; Krn, Keren. Bars, 10 µm.

pMad staining or PH3$^+$ number (Fig. 7 I). Similarly, expression of *dpp* RNAi in ECs using *Myo1A*-Gal4 (Fig. S5 N) or in midgut progenitors using *esg*-Gal4 (Fig. S5 O) had no effect on pMad staining or PH3$^+$ number (Fig. 7 I). Knockdown of *dpp* by *vm*-Gal4 for 8 d, however, resulted in a dramatic increase in PH3$^+$ cell number as compared with *vm*-Gal4 driving expression of GFP only (Fig. 7 I). Together, our data demonstrate that muscle-derived Dpp is the functionally relevant source of ligand that acts locally to initiate and maintain BMP signaling.

JAK-STAT signaling can induce BMP signaling in midgut epithelium

Because midgut injury induces JAK-STAT ligand expression in ECs (Jiang et al., 2009) and induces pMad and *Dad-lacZ* expression in midgut epithelia, we asked whether ectopic activation of the JAK-STAT signaling pathway alone could induce BMP signaling in midgut epithelium. Driving expression of UAS-*unpaired* (*upd*) in ECs using *Myo1A*^{ts} (Jiang et al., 2009) led to a dramatic increase in the expression of pMad in the midgut, suggesting that the injury-induced JAK-STAT signaling activates BMP ligand expression (Fig. 8, A and A′). Consistent with this model, ectopic activation of JAK-STAT signaling in circular muscle by *dpp*^{gut}*>hop*^{Tum} (a constitutively active form of the *Drosophila* JAK; Yan et al., 1996) resulted in pMad staining in midgut epithelium (Fig. 8 B).

Because ectopic expression of *upd* results in increased ISC proliferation, we considered the possibility that dividing ISCs were the source of signals that induce Dpp in the muscle after injury. Recently, it has been shown that *upd* is required for ISC maintenance (Osman et al., 2012). We reasoned that if ISCs were required for the induction of Dpp, we would fail to see activation of BMP signaling in the midgut after bleomycin treatment in intestines lacking ISCs. Although expressing *upd* RNAi in ISCs and EBs, using *esg*^{ts}, led to ISC loss in the anterior midgut, it had no effect on pMad staining in ECs after injury (Fig. 8, C and C′), suggesting that ECs, and not ISCs, are the source of signals that induce Dpp in vm (Fig. 8 D).

Discussion

To understand the active to quiescent transition of ISC proliferation after injury, we examined the role of the BMP signaling pathway in the *Drosophila* adult intestine. Midgut injury induces expression of JAK-STAT signaling ligands and EGFR signaling ligands in ECs. These ligands act directly on ISCs to increase their rate of proliferation and on vm to up-regulate Vein expression, which also acts on ISCs to promote stem cell division (Lucchetta and Ohlstein, 2012). Concomitantly, injury induces expression of Dpp in vm. Dpp constrains stem cell number and stem cell proliferation rate by directly activating BMP signaling in ISCs (Fig. 8 D). Thus, to meet the local needs of the midgut, local injury-induced BMP signaling, in conjunction with promitotic signals, modulates the ISC response to ensure the proper balance of signals to achieve an optimal response to injury.

Recently, Li et al. (2013) characterized the role of BMP signaling in the *Drosophila* adult midgut and reported that loss of BMP signaling in ECs results in widespread EC death, secretion of JAK-STAT and EGFR signaling ligands by dying cells, and a subsequent nonautonomous increase in ISC proliferation. However, using the same *Myo1A*^{ts} Gal4 driver and UAS-*tkv* and UAS-*Mad* RNAi stocks, we did not observe ISC overproliferation, even though we did see knockdown of *Dad-LacZ* and pMad expression. In addition, although Li et al. (2013) argued that tracheal-derived Dpp activates BMP signaling in ECs, we did not observe a decrease in pMad staining by driving two different *dpp* RNAi in trachea cells using the same *btl*-Gal4 driver as well as a new tracheal-specific driver *14D03*-Gal4. We did find that expressing *dpp* RNAi in vm using two different Gal4 drivers resulted in a decrease in pMad staining, dramatic increases in PH3 cell number, and a severe disruption in midgut homeostasis. Furthermore, the model proposed by Li et al. (2013) predicts that all ECs should be BMP signaling positive. Our results using two specific BMP signaling reporters demonstrate that, in the anterior and posterior midgut, many ECs are BMP signaling negative. Rather, only when the gut is severely injured do most ECs become BMP signaling positive, suggesting that BMP signaling pathway activation in the anterior and posterior midgut depends on a locally induced BMP signaling pathway ligand, rather than a constitutive ligand provided by trachea. Our results, therefore, argue that the functionally relevant source of Dpp is vm and not trachea.

A role for BMP signaling in patterning gut epithelium is conserved in vertebrates where the *dpp* homologue BMP 4 activates *Hox* genes to pattern the intestine (Roberts et al., 1995). Although BMP signaling is required for regional specification of the *Drosophila* midgut, whole midgut injury results in the activation of BMP signaling in the anterior and posterior midgut. Yet copper cells are not generated, demonstrating that BMP signaling is not sufficient for copper cell specification. The fact that BMP signaling outside the CCR does not result in ectopic production of copper cells suggests that the ability of BMP ligands to transform cell identity may depend on other yet unidentified regionally expressed cofactors.

JP syndrome patients harbor BMP signaling mutations (Houlston et al., 1998; Howe et al., 1998, 2001), and blocking BMP signaling in the mouse intestine generates a JP-like syndrome (Haramis et al., 2004; He et al., 2004). The main characteristics in JP syndrome are extensive generation of new crypts and increased cellular proliferation (Roth and Helwig, 1963; Haramis et al., 2004). Although BMP signaling ligands suppress sporadic colorectal cancer growth (Hardwick et al., 2004; Beck et al., 2006; Loh et al., 2008), and 70% of colorectal cancers fail to stain positive for various pSMads (Kodach et al., 2008), mutants in BMP signaling components have not been implicated in the initiation of intestinal adenomas (Hardwick et al., 2008). Based on our data, we would argue that BMP signaling acts as a modulator of the injury response. In states of high injury, BMP signaling loss would lead to an increase in stem cells, resulting in de novo crypt formation and hamartomas. As ISC number increases, so would the number of target cells available to acquire mutations in genes implicated in intestinal cancer, such as *APC* (*Adenomatous polyposis coli*) and *KRas*, thereby hastening the development of hamartomas into adenomas (Hardwick et al., 2008).

Materials and methods

Fly genetics

All *Drosophila* experimental stocks and crosses (except for RNAi ectopic expression) were cultured with daily changes of cornmeal food (referred to as control food) without live yeast at 23–25°C. Information regarding nomenclature and other relevant information on stocks used can be found at FlyBase.

Mutant and WT controls

Mutant and WT controls were *tkv*^{8} *FRT40A* (an amorphic allele with amino acid replacement C144@; the predicted product terminates immediately N-terminal to the conserved cysteine cluster in the extracellular domain; obtained from A. Spradling, Carnegie Institution of Washington, Washington, DC; Xie and Spradling, 1998), *tkv*^{4} *FRT 40A* (an amorphic allele with amino acid replacement W476@; obtained from R. Mann, Columbia University, New York, NY; Nellen et al., 1994), *Mad*^{12} *FRT40A* (an amorphic allele with amino acid replacement Q417@; obtained from G. Struhl, Columbia University, New York, NY; Xie and Spradling, 1998), *FRT82B punt*^{135} (amino acid replacement A376T; the point mutation is within the kinase domain; obtained from T. Xie, Stowers Institute for Medical Research, Kansas City, MO; Xie and Spradling, 1998), *FRT82B Dad*^{212} (a genetic null allele, in which an imprecise excision has generated a deletion that has removed three exons from the Dad gene, corresponding to amino acids 1–391; obtained from T. Tabata, University of Tokyo, Tokyo, Japan; Ogiso et al., 2011), *FRT82B ry*^{506} (Bloomington Stock Center [BL] #2035), and *FRT40A* (BL#1835).

Reporters and Gal4 drivers

Reporters and drivers used were *Dad*-lacZ (a lacZ transgene inserted into *Dad* that acts as a reporter of Dad expression; obtained from R. Xi, National Institute of Biological Science, Beijing, China; Tsuneizumi et al., 1997; Zhao et al., 2008), *upd3-Gal4 UAS-GFP/Cyo* (a *upd3* enhancer region-GAL4 fusion and a UAS-GFP reporter; obtained from N. Perrimon, Harvard Medical School, Boston, MA; Agaisse et al., 2003), *Gbe+ Su(H)LacZ* (*NRE-lacZ*; three copies of the grh protein binding element Gbe and two Su(H) binding sites from the E(spl) gene are fused upstream of a minimal Hsp70Bb promoter driving Ecol\lacZ expression; obtained from N. Perrimon; Micchelli and Perrimon, 2006), *tub-Gal80*^{ts}*/FM7; Su(H)Gbe-Gal4* (*NRE-Gal4*^{ts}; three copies of a grh protein binding element Gbe and two copies of Su(H) binding site drive expression of Scer\GAL4; Zeng et al., 2010), *esg-GFP* (Flytrap P01986, a GFP fusion/trap in *esg*), *esg-Gal4 UAS-GFP* (an *esg* enhancer region-GAL4 fusion and a UAS-GFP reporter; obtained from M. Markstein, University of Massachusetts, Amherst, MA), *esg-Gal4 UAS-GFP tub-Gal80/Cyo* (obtained from M. Markstein; Micchelli and Perrimon, 2006), *Dl-Gal4* (a putative *Dl* enhancer Gal4; BL#45136), *tub-Gal80*^{ts}*/Cyo, Myo1A-Gal4 tub-Gal80*^{ts} *UAS-GFP/Cyo* (from K. Irvine, Rutgers University, New Brunswick, NJ; Jiang et al., 2009), *tub-Gal80*^{ts}*/FM7;*

btl-Gal4 UAS-GFP (a *btl* promoter region-Gal4 fusion and a UAS-GFP reporter), *vm-Gal4* (a putative *hairy* enhancer Gal4; BL#48547; *tub>gal80>STOP* obtained from K. Scott, University of California, Berkeley, Berkeley, CA), *tub>gal80>STOP*; *UAS*-GFP, *vm-Gal4*, *dpp-Gal4^{gut}* (a putative *dpp* enhancer Gal4; strong; BL#45111), *dpp-Gal4^{gut}* (a putative *dpp* enhancer Gal4; weak; BL#47479), *14D03-Gal4* (a putative *trachealess* enhancer Gal4; BL#47463), and *dpp-LacZ* (*P* element construct P{PZ} inserted into the gene region of *dpp* acting as an enhancer trap; BL#12379).

MARCM stocks

MARCM 40A stock was yw hs-flp UAS-GFP; tub-Gal80 FRT40A; tub-Gal4/TM6B, Tb yw hs-flp; tub-Gal80 FRT 40A; tub-Gal4 UAS-dsRed/TM6B, Hu, and MARCM 82B stock was yw hs-flp tub-Gal4 UAS-dsRed;; FRT 82B tub-Gal80/TM3, Ser.

RNAi and ectopic expression stocks

Stocks used in this paper were *UAS-Mad RNAi* (BL#31315), *UAS-Mad RNAi* (Vienna Drosophila RNAi Center [V] #12635), and *UAS-Mad RNAi* (V#110517; all three lines produce similar phenotypes, but the strength is variable: BL#31315 > V#12635 > V#110517), *UAS-tkv RNAi* (V#3059), *UAS-dpp RNAi* (BL#25782), *UAS-dpp RNAi* (BL#33618), *UAS-Stat92E RNAi* (BL#31318), *UASp-tkv^{CA}* (Guo and Wang, 2009), *UAS-Ras^{N17}* (*UAS-Ras^{DN}*; BL#4846), *UAS-upd* (Tulina and Matunis, 2001), *UAS-hop^{Tum}* (Silver et al., 2005), and *UAS-upd RNAi* (V#3282).

Immunohistochemistry and microscopy

All samples were dissected in 2× gut buffer (200 mM glutamic acid, 50 mM KCl, 40 mM $MgSO_4$, 4 mM NaP monobasic, 4 mM NaP dibasic, and 2 mM $MgCl_2$; Ohlstein and Spradling, 2007) and fixed in 4% formaldehyde for 1 h. Primary antibodies were used at the following dilutions: rabbit anti–β-galactosidase at 1:10,000 (Cappel); guinea pig anti-pMAD at 1:1,000 (obtained from E. Laufer, Columbia University, New York, NY; Nahmad and Stathopoulos, 2009); guinea pig anti-Labial at 1:1,000; chicken anti-GFP at 1:10,000 (Abcam); mouse anti-Prospero at 1:100 (MR1A; Developmental Studies Hybridoma Bank); mouse anti-Dl at 1:100 (C594.9B; Developmental Studies Hybridoma Bank); rabbit anti-Pdm1 at 1:500 (Lee et al., 2009); and rabbit anti–phospho-histone H3 (1:10,000; #3377; Cell Signaling Technology). Alexa Fluor–conjugated secondary antibodies were used at 1:4,000 (Molecular Probes and Invitrogen). Guts were stained with 1 µg/ml DAPI (Sigma-Aldrich), mounted in 70% glycerol, and imaged with a spinning-disc confocal microscope (DSU; Olympus) using UPLFLN 20×, 40× oil, and 60× oil objectives (imaging medium: immersion oil type F obtained from Olympus). The imaging temperature was at room temperature. The camera used was an electron multiplying charge-coupled device camera (ImagEM Enhanced C9100-13; Hamamatsu Photonics). The acquisition and processing software was SlideBook (version 4.2; Intelligent Imaging Innovations). Images were processed in Photoshop CS5 (Abode) and Illustrator CS4 (Adobe) for image merging and resizing.

MARCM ISC mosaic analysis

For *tkv^{8} FRT40A*, *tkv^{4} FRT40A*, and *Mad^{12} FRT40A* ISC MARCM clonal analysis, *FRT40A* (BL#1835) was used as a WT control. Because *Dad* mutants were present on a chromosome containing FRT82B, we chose to use FRT82B *ry^{506}* as a WT control and the type II BMP receptor mutant *punt^{135}*, also present on a chromosome containing FRT82B, to knockdown BMP signaling. *UAS-Stat92E RNAi*, *UAS-tkv^{CA}*, and *UAS-Ras^{DN}* were combined with *FRT40A* (BL#1835) to make MARCM clones.

To induce ISC MARCM clones, 3-d-old adult female flies were heat shocked in empty vials at 37°C for 40 min in a water bath and then transferred daily to new cornmeal food without live yeast. GFP- or RFP-labeled ISC MARCM clones were analyzed at various time points ACI as described in the Results or figure legends.

Labial antibody production

A 924-bp fragment of the *labial* gene was amplified from cDNA using primers forward, 5′-ATGTACACCAACCTGGACTGC-3′, and reverse, 5′-TCAGGTCAGCTGCTTGTTGGTGAA-3′, with the reverse primer having an added stop codon (underlined). The PCR fragment was cloned into the vector pCR8/GW/TOPO (Invitrogen), subcloned into the protein expression vector pDEST17 (Invitrogen), and then used to transform BL21A competent cells. 6×His-tagged protein was purified from lysate using Ni–nitrilotriacetic acid flow columns (QIAGEN) and was injected into guinea pig (Covance). Sera were collected over a period of 2 mo and tested for specificity by Western blot analysis.

Bromophenol blue dye feeding

A 1-ml solution of 0.15% bromophenol blue was added to 0.5 g of dry yeast resulting in a yeast paste. Animals were fed this yeast paste for 5–8 h, and midguts were dissected and analyzed as described in Fig. 1 (H and I) and Fig. S1 G.

Bleomycin, paraquat treatment, and *ECC15* infection

Chromatography paper (Fisherbrand; Thermo Fisher Scientific) was cut into 3.7 × 5.8–cm strips and saturated with 25 µg/ml bleomycin (Sigma-Aldrich) or 10 mM paraquat (Sigma-Aldrich) dissolved in 5% sucrose. Bacteria *ECC15* were cultured overnight in Lysogeny broth medium containing antibiotics (100 µg/ml rifampicin and 600 µg/ml carbenicillin). A concentrated bacterial pellet (OD of ≈600), which was centrifuged from 1-ml overnight culture media, was dissolved in 1-ml 5% sucrose.

Before treatment, flies were starved in empty vials for 1 h and then transferred into vials with bleomycin-, paraquat-, or *ECC15* solution–saturated paper. After 24 h of treatment, flies were transferred daily to new cornmeal food.

TUNEL assay

Guts were fixed in 4% formaldehyde/gut buffer for 1 h, washed 30 min with PBS, incubated in permeabilization solution for 2 min on ice, washed with PBS, and then incubated in a mixture of enzyme and label solutions (Roche kit) at 37°C for 3 h in a dark humidified chamber. After three washes with PBS, guts were mounted in 70% glycerol.

Ectopic *RNAi* expression

Knocking down BMP signaling during embryo or larval stage usually causes lethality before fly eclosion. Midgut drivers combined with temperature-inducible *tub-Gal80^{ts}* (Jiang et al., 2009) were used to selectively ectopic express *Mad*, *tkv*, and *dpp RNAi* in *Drosophila* adults as described in Fig. 1 (H and I), Fig. 3 (J–L), Fig. 8 (A and C), Fig. S1 (B–D and G), Fig. S3 (G–K), and Fig. S5 (F and K–O). Flies were cultured at 18°C during development, and then, female adult flies were shifted to 30°C to induce ectopic expression of *RNAi* transgenes. To eliminate copper cells as described in Fig. 1, flies were cultured at room temperature, and then, female adult flies were shifted to 30°C to induce ectopic expression of *RNAi* transgenes. Midguts were analyzed at various time points after temperature shifts as described in the Results or figure legends.

Ablation of ISCs in the anterior midgut

esg^{ts}>upd RNAi (V#3282) flies were cultured at 18°C during development, and then, female adult flies were shifted to 30°C for 8 d to ablate ISCs.

Cell identification in mutant clones

We used the following criteria to identify stem cells: Dl-positive, *NRE-lacZ*–negative, and Prospero-negative diploid cells. *NRE-lacZ* expression (Choi et al., 2011) was used to identify EBs, Prospero was used to identify enteroendocrine cells (Micchelli and Perrimon, 2006; Ohlstein and Spradling, 2006), and nuclear size (Ohlstein and Spradling, 2006) was used to identify ECs.

Colcemid treatment

Fisherbrand chromatography paper strips were saturated with 200 µg/ml colcemid (Sigma-Aldrich) dissolved in 5% sucrose. 8 d ACI, *FRT40A*, *tkv^{8} FRT40A*, and *Mad^{12} FRT40A* MARCM flies were transferred into vials with colcemid-saturated paper. After 24 h of treatment, flies were dissected and stained with anti–phospho-histone H3 antibody.

Mosaic expression of *dpp RNAi* in muscle

Flies with the genotype *tub-FRT-Gal80-FRT/yw hs-flp; UAS-GFP; vm-Gal4/UAS-dpp RNAi* were collected and reared on cornmeal food at 25°C. The expression of Gal80 by the *tub* promoter prevents expression of the *vm-Gal4* driver, which is expressed in vm. Exposure of flies to heat shock temperatures leads to excision of the Gal80 cassette, which results in *vm-Gal4* expression. Depending on the length of heat shock, the Gal80 cassette will excise in a subset of muscle cells, leading to mosaic expression of UAS-*dpp* RNAi. 3 d after eclosion, mosaic expression was induced by a 30-min heat shock at 37°C in a water bath. Flies were then transferred to cornmeal food and reared at 25°C. Flies were treated with bleomycin from 7 d ACI to 8 d ACI. 8 d after induction, GFP-labeled mosaic ectopic expression of *dpp RNAi* in muscle was analyzed by staining for pMad and GFP.

***dpp* mRNA in situ by FISH**

48 single-labeled oligonucleotides designed to selectively bind to *dpp* mRNA transcripts were purchased from Biosearch Technologies (Custom

Stellaris FISH Probes). Dried oligonucleotide probes were dissolved in 200 µl of TE (Tris and EDTA) buffer, resulting in a probe stock with a total oligonucleotide concentration of 25 µM. 20 µl of probe stock solution was added to 80 µl TE buffer and used as a source of working probe solution. Fixation solution was 3.7% formaldehyde in PBS. Hybridization buffer was 100 mg/ml dextran sulfate and 10% formamide in 2× SSC. Wash buffer was 10% formamide in 2× SSC. 1 µl of working probe solution was mixed with 100 µl hybridization buffer to create the hybridization solution.

Flies were fed with bleomycin for 24 h followed by dissection. Midguts were fixed with fixation solution for 45 min and then washed twice with PBS. Hybridization protocol is as follows: (a) add 1 ml of 70% EtOH to fixed midguts and store overnight at 4°C in a covered glass chamber; (b) aspirate the 70% EtOH from the sample; (c) add 1 ml of wash buffer and let stand for 2–5 min; (d) aspirate the wash buffer and add 100 µl hybridization solution; (e) incubate in the dark in a water bath at 37°C overnight; (f) add 1 ml wash buffer and incubate in the dark in a water bath at 37°C for 30 min; (g) aspirate the wash buffer and stain with DAPI in new 1 ml wash buffer; and (h) proceed to imaging.

RT-qPCR

esg-Gal4 UAS-GFP flies were used as RT-qPCR sample flies. For each RT-qPCR, 60 newly eclosed female flies were collected for 2 d, aged for an additional 3 d, and then equally split into two groups. One group of flies was fed 25 ng/ml bleomycin, and the other group was transferred into cornmeal food as a control. After 24 h of treatment, midguts were dissected from flies and kept in Schneider's media with 10% FBS before RNA extraction.

RNeasy Mini kit (QIAGEN) was used to obtain midgut RNA. RNA samples were reverse transcribed into cDNA using cDNA SuperMix (qScript; Quanta BioSciences). RT-qPCR was then performed in duplicate for each cDNA sample.

RNA preparation was repeated three times. *upd3*, *dpp*, and *Dad* mRNA expression levels were normalized against mRNA levels of *Rp49*. Three sets of data were analyzed by Student's *t* tests between control RNA and bleomycin-treated RNA. Primers used in this RT-qPCR are listed as follows: Rp49 forward primer, 5′-GGCCCAAGATCGTGAAGAAG-3′, and reverse primer, 5′-CTGTTCCTCGCTGCACTTTA-3′; upd3 forward primer, 5′-CCCAGCCAACGATTTTTATG-3′, and reverse primer, 5′-TGTTACCGCTCCGGCTAC-3′; dpp forward primer, 5′-GCCAACACAGTGCGAAGTT-3′, and reverse primer, 5′-ACCACCTGTTGACTGAGTGC-3′; and Dad forward primer, 5′-GCATCCTGCACCAGCCCGAAACA-3′, and reverse primer, 5′-CGTGCTGAGCGCTGCCGACTTTG-3′.

Statistical analysis

MARCM clone sizes and $PH3^+$ cell number were plotted as individual values. Error bars in Fig. 5 (H and I) and Fig.7 A are SEM. Statistics were performed using one-way analysis of variance (ANOVA) test on Prism (GraphPad Software). Significance was accepted at *, $P < 0.01$; **, $P < 0.001$; and ***, $P < 0.0001$.

Online supplemental material

Fig. S1 shows coexpression of *Dad*-lacZ and the enteroendocrine marker prospero and that BMP signaling is required in progenitors for copper cell differentiation. Fig. S2 shows up-regulation of *Dad*-lacZ expression after paraquat and bleomycin treatment. Fig. S3 shows loss of pMad and *Dad*-lacZ expression in BMP mutant clones in the anterior and posterior midgut, TUNEL labeling in Mad mutant clones, Dl-Gal4 expression the CCR, and the loss of pMad and *Dad*–lacZ expression after knockdown of BMP signaling in ECs. Fig. S4 shows up-regulation of pMad expression in cells in which BMP signaling is constitutively active and a diagram outlining the experimental approach to determine the effect of loss of BMP signaling and activation of BMP signaling on clone growth before and after injury. Fig. S5 shows that Dpp is required in vm to regulate midgut homeostasis. Online supplemental material is available at http://www.jcb.org/cgi/content/full/jcb.201302049/DC1. Additional data are available in the JCB DataViewer at http://dx.doi.org/10.1083/jcb.201302049.dv.

The authors would like to thank the following for providing reagents: A. Spradling, E. Laufer, R. Mann, G. Struhl, T. Tabata, R. Xi, N. Perrimon, B. Edgar, T. Xie, M. Markstein, K. Irvine, and K. Scott.

I. Driver was supported in part by 5-T32-HD055165-01. This work was supported by National Institutes of Health grant R01 DK082456-01 to B. Ohlstein.

Submitted: 11 February 2013
Accepted: 29 April 2013

References

Adachi-Yamada, T., M. Nakamura, K. Irie, Y. Tomoyasu, Y. Sano, E. Mori, S. Goto, N. Ueno, Y. Nishida, and K. Matsumoto. 1999. p38 mitogen-activated protein kinase can be involved in transforming growth factor beta superfamily signal transduction in *Drosophila* wing morphogenesis. *Mol. Cell. Biol.* 19:2322–2329.

Agaisse, H., U.M. Petersen, M. Boutros, B. Mathey-Prevot, and N. Perrimon. 2003. Signaling role of hemocytes in *Drosophila* JAK/STAT-dependent response to septic injury. *Dev. Cell*. 5:441–450. http://dx.doi.org/10.1016/S1534-5807(03)00244-2

Amcheslavsky, A., J. Jiang, and Y.T. Ip. 2009. Tissue damage-induced intestinal stem cell division in *Drosophila*. *Cell Stem Cell*. 4:49–61. http://dx.doi.org/10.1016/j.stem.2008.10.016

Basset, A., R.S. Khush, A. Braun, L. Gardan, F. Boccard, J.A. Hoffmann, and B. Lemaitre. 2000. The phytopathogenic bacteria *Erwinia carotovora* infects *Drosophila* and activates an immune response. *Proc. Natl. Acad. Sci. USA*. 97:3376–3381. http://dx.doi.org/10.1073/pnas.97.7.3376

Beck, S.E., B.H. Jung, A. Fiorino, J. Gomez, E.D. Rosario, B.L. Cabrera, S.C. Huang, J.Y. Chow, and J.M. Carethers. 2006. Bone morphogenetic protein signaling and growth suppression in colon cancer. *Am. J. Physiol. Gastrointest. Liver Physiol.* 291:G135–G145. http://dx.doi.org/10.1152/ajpgi.00482.2005

Beebe, K., W.C. Lee, and C.A. Micchelli. 2010. JAK/STAT signaling coordinates stem cell proliferation and multilineage differentiation in the *Drosophila* intestinal stem cell lineage. *Dev. Biol.* 338:28–37. http://dx.doi.org/10.1016/j.ydbio.2009.10.045

Biteau, B., and H. Jasper. 2011. EGF signaling regulates the proliferation of intestinal stem cells in *Drosophila*. *Development*. 138:1045–1055. http://dx.doi.org/10.1242/dev.056671

Biteau, B., C.E. Hochmuth, and H. Jasper. 2008. JNK activity in somatic stem cells causes loss of tissue homeostasis in the aging *Drosophila* gut. *Cell Stem Cell*. 3:442–455. http://dx.doi.org/10.1016/j.stem.2008.07.024

Buchon, N., N.A. Broderick, S. Chakrabarti, and B. Lemaitre. 2009. Invasive and indigenous microbiota impact intestinal stem cell activity through multiple pathways in *Drosophila*. *Genes Dev.* 23:2333–2344. http://dx.doi.org/10.1101/gad.1827009

Buchon, N., N.A. Broderick, T. Kuraishi, and B. Lemaitre. 2010. *Drosophila* EGFR pathway coordinates stem cell proliferation and gut remodeling following infection. *BMC Biol.* 8:152. http://dx.doi.org/10.1186/1741-7007-8-152

Buszczak, M., S. Paterno, D. Lighthouse, J. Bachman, J. Planck, S. Owen, A.D. Skora, T.G. Nystul, B. Ohlstein, A. Allen, et al. 2007. The carnegie protein trap library: a versatile tool for *Drosophila* developmental studies. *Genetics*. 175:1505–1531. http://dx.doi.org/10.1534/genetics.106.065961

Chatterjee, M., and Y.T. Ip. 2009. Pathogenic stimulation of intestinal stem cell response in *Drosophila*. *J. Cell. Physiol.* 220:664–671. http://dx.doi.org/10.1002/jcp.21808

Choi, N.H., J.G. Kim, D.J. Yang, Y.S. Kim, and M.A. Yoo. 2008. Age-related changes in *Drosophila* midgut are associated with PVF2, a PDGF/VEGF-like growth factor. *Aging Cell*. 7:318–334. http://dx.doi.org/10.1111/j.1474-9726.2008.00380.x

Choi, N.H., E. Lucchetta, and B. Ohlstein. 2011. Nonautonomous regulation of *Drosophila* midgut stem cell proliferation by the insulin-signaling pathway. *Proc. Natl. Acad. Sci. USA*. 108:18702–18707. http://dx.doi.org/10.1073/pnas.1109348108

Chouinard, S., and T.C. Kaufman. 1991. Control of expression of the homeotic labial (lab) locus of *Drosophila melanogaster*: evidence for both positive and negative autogenous regulation. *Development*. 113:1267–1280.

Dubreuil, R.R. 2004. Copper cells and stomach acid secretion in the *Drosophila* midgut. *Int. J. Biochem. Cell Biol.* 36:742–752. http://dx.doi.org/10.1016/j.biocel.2003.07.004

Dubreuil, R.R., J. Frankel, P. Wang, J. Howrylak, M. Kappil, and T.A. Grushko. 1998. Mutations of alpha spectrin and labial block cuprophilic cell differentiation and acid secretion in the middle midgut of *Drosophila* larvae. *Dev. Biol.* 194:1–11. http://dx.doi.org/10.1006/dbio.1997.8821

Filshie, B.K., D.F. Poulson, and D.F. Waterhouse. 1971. Ultrastructure of the copper-accumulating region of the *Drosophila* larval midgut. *Tissue Cell*. 3:77–102. http://dx.doi.org/10.1016/S0040-8166(71)80033-2

Guo, Z., and Z. Wang. 2009. The glypican Dally is required in the niche for the maintenance of germline stem cells and short-range BMP signaling in the *Drosophila* ovary. *Development*. 136:3627–3635. http://dx.doi.org/10.1242/dev.036939

Haramis, A.P., H. Begthel, M. van den Born, J. van Es, S. Jonkheer, G.J. Offerhaus, and H. Clevers. 2004. De novo crypt formation and juvenile polyposis on BMP inhibition in mouse intestine. *Science*. 303:1684–1686. http://dx.doi.org/10.1126/science.1093587

Hardwick, J.C., G.R. Van Den Brink, S.A. Bleuming, I. Ballester, J.M. Van Den Brande, J.J. Keller, G.J. Offerhaus, S.J. Van Deventer, and M.P. Peppelenbosch. 2004. Bone morphogenetic protein 2 is expressed by, and acts upon, mature epithelial cells in the colon. *Gastroenterology*. 126:111–121. http://dx.doi.org/10.1053/j.gastro.2003.10.067

Hardwick, J.C., L.L. Kodach, G.J. Offerhaus, and G.R. van den Brink. 2008. Bone morphogenetic protein signalling in colorectal cancer. *Nat. Rev. Cancer*. 8:806–812. http://dx.doi.org/10.1038/nrc2467

He, X.C., J. Zhang, W.G. Tong, O. Tawfik, J. Ross, D.H. Scoville, Q. Tian, X. Zeng, X. He, L.M. Wiedemann, et al. 2004. BMP signaling inhibits intestinal stem cell self-renewal through suppression of Wnt-beta-catenin signaling. *Nat. Genet.* 36:1117–1121. http://dx.doi.org/10.1038/ng1430

Hochmuth, C.E., B. Biteau, D. Bohmann, and H. Jasper. 2011. Redox regulation by Keap1 and Nrf2 controls intestinal stem cell proliferation in *Drosophila*. *Cell Stem Cell*. 8:188–199. http://dx.doi.org/10.1016/j.stem.2010.12.006

Hoppler, S., and M. Bienz. 1994. Specification of a single cell type by a *Drosophila* homeotic gene. *Cell*. 76:689–702. http://dx.doi.org/10.1016/0092-8674(94)90508-8

Houlston, R., S. Bevan, A. Williams, J. Young, M. Dunlop, P. Rozen, C. Eng, D. Markie, K. Woodford-Richens, M.A. Rodriguez-Bigas, et al. 1998. Mutations in DPC4 (SMAD4) cause juvenile polyposis syndrome, but only account for a minority of cases. *Hum. Mol. Genet.* 7:1907–1912. http://dx.doi.org/10.1093/hmg/7.12.1907

Howe, J.R., S. Roth, J.C. Ringold, R.W. Summers, H.J. Järvinen, P. Sistonen, I.P. Tomlinson, R.S. Houlston, S. Bevan, F.A. Mitros, et al. 1998. Mutations in the SMAD4/DPC4 gene in juvenile polyposis. *Science*. 280:1086–1088. http://dx.doi.org/10.1126/science.280.5366.1086

Howe, J.R., J.L. Bair, M.G. Sayed, M.E. Anderson, F.A. Mitros, G.M. Petersen, V.E. Velculescu, G. Traverso, and B. Vogelstein. 2001. Germline mutations of the gene encoding bone morphogenetic protein receptor 1A in juvenile polyposis. *Nat. Genet.* 28:184–187. http://dx.doi.org/10.1038/88919

Jiang, H., and B.A. Edgar. 2009. EGFR signaling regulates the proliferation of *Drosophila* adult midgut progenitors. *Development*. 136:483–493. http://dx.doi.org/10.1242/dev.026955

Jiang, H., P.H. Patel, A. Kohlmaier, M.O. Grenley, D.G. McEwen, and B.A. Edgar. 2009. Cytokine/Jak/Stat signaling mediates regeneration and homeostasis in the *Drosophila* midgut. *Cell*. 137:1343–1355. http://dx.doi.org/10.1016/j.cell.2009.05.014

Jiang, H., M.O. Grenley, M.-J. Bravo, R.Z. Blumhagen, and B.A. Edgar. 2011. EGFR/Ras/MAPK signaling mediates adult midgut epithelial homeostasis and regeneration in *Drosophila*. *Cell Stem Cell*. 8:84–95. http://dx.doi.org/10.1016/j.stem.2010.11.026

Jiang, J., and G. Struhl. 1995. Protein kinase A and hedgehog signaling in *Drosophila* limb development. *Cell*. 80:563–572. http://dx.doi.org/10.1016/0092-8674(95)90510-3

Karpowicz, P., J. Perez, and N. Perrimon. 2010. The Hippo tumor suppressor pathway regulates intestinal stem cell regeneration. *Development*. 137:4135–4145. http://dx.doi.org/10.1242/dev.060483

Kodach, L.L., E. Wiercinska, N.F. de Miranda, S.A. Bleuming, A.R. Musler, M.P. Peppelenbosch, E. Dekker, G.R. van den Brink, C.J. van Noesel, H. Morreau, et al. 2008. The bone morphogenetic protein pathway is inactivated in the majority of sporadic colorectal cancers. *Gastroenterology*. 134:1332–1341. http://dx.doi.org/10.1053/j.gastro.2008.02.059

König, A., A.S. Yatsenko, M. Weiss, and H.R. Shcherbata. 2011. Ecdysteroids affect *Drosophila* ovarian stem cell niche formation and early germline differentiation. *EMBO J.* 30:1549–1562. http://dx.doi.org/10.1038/emboj.2011.73

Lee, T., and L. Luo. 1999. Mosaic analysis with a repressible cell marker for studies of gene function in neuronal morphogenesis. *Neuron*. 22:451–461. http://dx.doi.org/10.1016/S0896-6273(00)80701-1

Lee, W.C., K. Beebe, L. Sudmeier, and C.A. Micchelli. 2009. Adenomatous polyposis coli regulates *Drosophila* intestinal stem cell proliferation. *Development*. 136:2255–2264. http://dx.doi.org/10.1242/dev.035196

Li, Z., Y. Zhang, L. Han, L. Shi, and X. Lin. 2013. Trachea-derived dpp controls adult midgut homeostasis in *Drosophila*. *Dev. Cell*. 24:133–143. http://dx.doi.org/10.1016/j.devcel.2012.12.010

Lin, G., N. Xu, and R. Xi. 2010. Paracrine unpaired signaling through the JAK/STAT pathway controls self-renewal and lineage differentiation of drosophila intestinal stem cells. *J. Mol. Cell Biol*. 2:37–49. http://dx.doi.org/10.1093/jmcb/mjp028

Loh, K., J.A. Chia, S. Greco, S.J. Cozzi, R.L. Buttenshaw, C.E. Bond, L.A. Simms, T. Pike, J.P. Young, J.R. Jass, et al. 2008. Bone morphogenic protein 3 inactivation is an early and frequent event in colorectal cancer development. *Genes Chromosomes Cancer*. 47:449–460. http://dx.doi.org/10.1002/gcc.20552

Lucchetta, E.M., and B. Ohlstein. 2012. The *Drosophila* midgut: a model for stem cell driven tissue regeneration. *WIREs Dev. Biol*. 1:781–788. http://dx.doi.org/10.1002/wdev.51

Micchelli, C.A., and N. Perrimon. 2006. Evidence that stem cells reside in the adult *Drosophila* midgut epithelium. *Nature*. 439:475–479. http://dx.doi.org/10.1038/nature04371

Nahmad, M., and A. Stathopoulos. 2009. Dynamic interpretation of hedgehog signaling in the *Drosophila* wing disc. *PLoS Biol.* 7:e1000202. http://dx.doi.org/10.1371/journal.pbio.1000202

Nellen, D., M. Affolter, and K. Basler. 1994. Receptor serine/threonine kinases implicated in the control of *Drosophila* body pattern by decapentaplegic. *Cell*. 78:225–237. http://dx.doi.org/10.1016/0092-8674(94)90293-3

Ogiso, Y., K. Tsuneizumi, N. Masuda, M. Sato, and T. Tabata. 2011. Robustness of the Dpp morphogen activity gradient depends on negative feedback regulation by the inhibitory Smad, Dad. *Dev. Growth Differ.* 53:668–678. http://dx.doi.org/10.1111/j.1440-169X.2011.01274.x

Ohlstein, B., and A. Spradling. 2006. The adult *Drosophila* posterior midgut is maintained by pluripotent stem cells. *Nature*. 439:470–474. http://dx.doi.org/10.1038/nature04333

Ohlstein, B., and A. Spradling. 2007. Multipotent *Drosophila* intestinal stem cells specify daughter cell fates by differential notch signaling. *Science*. 315:988–992. http://dx.doi.org/10.1126/science.1136606

Osman, D., N. Buchon, S. Chakrabarti, Y.T. Huang, W.C. Su, M. Poidevin, Y.C. Tsai, and B. Lemaitre. 2012. Autocrine and paracrine unpaired signaling regulate intestinal stem cell maintenance and division. *J. Cell Sci.* 125:5944–5949. http://dx.doi.org/10.1242/jcs.113100

Panganiban, G.E., R. Reuter, M.P. Scott, and F.M. Hoffmann. 1990. A *Drosophila* growth factor homolog, decapentaplegic, regulates homeotic gene expression within and across germ layers during midgut morphogenesis. *Development*. 110:1041–1050.

Pfeiffer, B.D., A. Jenett, A.S. Hammonds, T.T. Ngo, S. Misra, C. Murphy, A. Scully, J.W. Carlson, K.H. Wan, T.R. Laverty, et al. 2008. Tools for neuroanatomy and neurogenetics in *Drosophila. Proc. Natl. Acad. Sci. USA*. 105:9715–9720. http://dx.doi.org/10.1073/pnas.0803697105

Roberts, D.J., R.L. Johnson, A.C. Burke, C.E. Nelson, B.A. Morgan, and C. Tabin. 1995. Sonic hedgehog is an endodermal signal inducing Bmp-4 and Hox genes during induction and regionalization of the chick hindgut. *Development*. 121:3163–3174.

Roth, S.I., and E.B. Helwig. 1963. Juvenile polyps of the colon and rectum. *Cancer*. 16:468–479. http://dx.doi.org/10.1002/1097-0142(196304)16:4<468::AID-CNCR2820160408>3.0.CO;2-F

Shanbhag, S., and S. Tripathi. 2009. Epithelial ultrastructure and cellular mechanisms of acid and base transport in the *Drosophila* midgut. *J. Exp. Biol.* 212:1731–1744. http://dx.doi.org/10.1242/jeb.029306

Shaw, R.L., A. Kohlmaier, C. Polesello, C. Veelken, B.A. Edgar, and N. Tapon. 2010. The Hippo pathway regulates intestinal stem cell proliferation during *Drosophila* adult midgut regeneration. *Development*. 137:4147–4158. http://dx.doi.org/10.1242/dev.052506

Silver, D.L., E.R. Geisbrecht, and D.J. Montell. 2005. Requirement for JAK/STAT signaling throughout border cell migration in *Drosophila. Development*. 132:3483–3492. http://dx.doi.org/10.1242/dev.01910

Staehling-Hampton, K., and F.M. Hoffmann. 1994. Ectopic decapentaplegic in the *Drosophila* midgut alters the expression of five homeotic genes, dpp, and wingless, causing specific morphological defects. *Dev. Biol.* 164:502–512. http://dx.doi.org/10.1006/dbio.1994.1219

Staley, B.K., and K.D. Irvine. 2010. Warts and Yorkie mediate intestinal regeneration by influencing stem cell proliferation. *Curr. Biol.* 20:1580–1587. http://dx.doi.org/10.1016/j.cub.2010.07.041

Strand, M., and C.A. Micchelli. 2011. Quiescent gastric stem cells maintain the adult *Drosophila* stomach. *Proc. Natl. Acad. Sci. USA*. 108:17696–17701. http://dx.doi.org/10.1073/pnas.1109794108

Tsuneizumi, K., T. Nakayama, Y. Kamoshida, T.B. Kornberg, J.L. Christian, and T. Tabata. 1997. Daughters against dpp modulates dpp organizing activity in *Drosophila* wing development. *Nature*. 389:627–631. http://dx.doi.org/10.1038/39362

Tulina, N., and E. Matunis. 2001. Control of stem cell self-renewal in *Drosophila* spermatogenesis by JAK-STAT signaling. *Science*. 294:2546–2549. http://dx.doi.org/10.1126/science.1066700

Wharton, K., and R. Derynck. 2009. TGFbeta family signaling: novel insights in development and disease. *Development*. 136:3691–3697. http://dx.doi.org/10.1242/dev.040584

Xie, T., and A.C. Spradling. 1998. decapentaplegic is essential for the maintenance and division of germline stem cells in the *Drosophila* ovary. *Cell*. 94:251–260. http://dx.doi.org/10.1016/S0092-8674(00)81424-5

Xu, N., S.Q. Wang, D. Tan, Y. Gao, G. Lin, and R. Xi. 2011. EGFR, Wingless and JAK/STAT signaling cooperatively maintain *Drosophila* intestinal stem cells. *Dev. Biol.* 354:31–43. http://dx.doi.org/10.1016/j.ydbio.2011.03.018

Yan, R., H. Luo, J.E. Darnell Jr., and C.R. Dearolf. 1996. A JAK-STAT pathway regulates wing vein formation in *Drosophila. Proc. Natl. Acad. Sci. USA*. 93:5842–5847. http://dx.doi.org/10.1073/pnas.93.12.5842

Zeng, X., C. Chauhan, and S.X. Hou. 2010. Characterization of midgut stem cell- and enteroblast-specific Gal4 lines in *Drosophila*. *Genesis*. 48:607–611. http://dx.doi.org/10.1002/dvg.20661

Zhao, R., Y. Xuan, X. Li, and R. Xi. 2008. Age-related changes of germline stem cell activity, niche signaling activity and egg production in *Drosophila. Aging Cell*. 7:344–354. http://dx.doi.org/10.1111/j.1474-9726.2008.00379.x